Paleoclimatic tracers: An investigation using an atmospheric general circulation model under ice age conditions - 2. Water isotopes

Sylvie Joussaume, Jean Jouzel

JOURNAL OF GEOPHYSICAL RESEARCH, VOL. 98, NO. D2, PAGES 2807–2830, FEBRUARY 20, 1993

Paleoclimatic Tracers: An Investigation Using an Atmospheric General Circulation Model Under Ice Age Conditions 2. Water Isotopes

SYLVIE JOUSSAUME[1]

Laboratoire de Météorologie Dynamique, Centre National de la Recherche Scientifique, Paris, France

JEAN JOUZEL[2]

Laboratoire de Modélisation du Climat et de l'Environnement, Commissariat à l'Energie Atomique, Saclay, France

The linear relationship observed between the water isotopic contents of precipitation and surface air temperatures leads to the use of the water isotopes, $H_2{}^{18}O$ and HDO, in paleoclimatology. Applied to the measurements of the isotopic content of paleowaters, like groundwaters and deep ice cores, this relationship is used to infer paleotemperatures. However, this interpretation of paleo-isotopic contents is only valid if the isotope-temperature relationship is not affected by climate change. To address this problem, we have developed a water isotope modeling inside an atmospheric general circulation model (AGCM) and performed simulations of both the present-day and Last Glacial Maximum (LGM) climatic conditions. AGCMs are indeed the only appropriate tools able to account the whole complexity of the atmospheric circulation. For the present-day climate, preliminary results for January were presented by Joussaume et al. (1984) and are complemented by new simulations performed for both February and August climatic conditions with a higher-resolution version of the model. Model results are well corroborated by observations. They also exhibit some effects of the atmospheric circulation on the isotopic fields. For the simulated LGM climate, the model results compare well with paleoclimatic data of water isotopic contents, except for a higher than observed spatial variability. The overall patterns of the simulated $\delta^{18}O$-temperature relationship for the LGM climate are practically unchanged, which tends to comfort the use of water isotopes in paleoclimatology. However, concerning the deuterium excess, i.e., the relationship between oxygen 18 and deuterium, the model results are not sufficiently valid to allow a discussion of the use of deuterium excess in paleoclimatology.

1. Introduction

Natural waters contain a very small amount of the heavier isotope species $H_2{}^{18}O$ and HDO. In the ocean, the mean isotopic ratios $H_2{}^{18}O/H_2{}^{16}O$ and $HDO/H_2{}^{16}O$ are not larger than 0.2% and 0.03% respectively. Although very small, these ratios lie at the heart of the use of water isotopes in paleoclimatology.

Observations for the present-day climate indicate a linear relationship between the isotopic content of precipitation and the surface air temperature, with lower isotopic ratios occurring at lower temperatures. This isotope-temperature relationship is well observed in the middle to high latitudes, both on a global scale [*Dansgaard,* 1964] and on a regional scale, e.g., over Antarctica [*Lorius and Merlivat,* 1977]. The measurement of the isotopic content of paleowaters, such as groundwater or ice from deep ice cores, should therefore allow the reconstruction of paleotemperatures [e.g., *Lorius et al.,* 1985]. However, this interpretation assumes that the isotope-temperature relationship is insensitive to climatic changes. A good understanding of the atmospheric cycle of the water isotopes is thus required.

The water isotope species have different saturation vapor pressures and molecular diffusivities, and these differences induce fractionation processes at each phase change. Due to the lower saturation pressures of the heavier water isotopes, the condensed phase is always enriched in these isotopes relative to the vapor phase. Moreover, the molecular exchanges between phases are also slowed down for heavier isotopes due to their weaker molecular diffusivities.

The basic mechanism behind the isotope-temperature relationship can then be explained as follows. Water vapor evaporates over the warm tropical waters with an isotopic content roughly in equilibrium with that in the underlying ocean. Then, during transport toward colder regions, this water vapor experiences successive condensations as the saturation vapor pressure decreases, resulting in a progressive depletion of the isotopic ratio of the remaining water vapor. Thus, the precipitation formed in isotopic equilibrium with the water vapor remaining at colder temperatures will have a lower isotopic content (Figure 1). This relationship is well understood and reproduced by simple isotopic models that are based on the thermodynamic evolution of an isolated air mass [*Dansgaard,* 1964; *Jouzel and Merlivat,* 1984].

However, simple isotopic models also show that the isotope-temperature relationship is sensitive to other factors, such as the trajectory of the air mass [*Dansgaard,* 1964] and the

[1] Now at Laboratoire de Modélisation du Climat et de l'Environnement, Commissariat à l'Energie Atomique, Gif-sur-Yvette, and also at Laboratoire d'Océanographie Dynamique et de Climatologie, Centre National de la Recherche Scientifique, Paris, France.

[2] Also at Laboratoire de Glaciologie et de Géophysique de l'Environnement, Centre National de la Recherche Scientifique, Grenoble, France.

Paper number 92JD01920.
0148-0227/93/92JD-01920$05.00

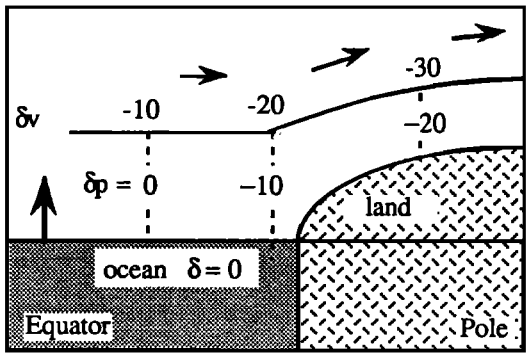

Fig. 1. Schematic representation of the atmospheric cycle of oxygen 18 content in vapor δ_v and in precipitation δ_p (adapted from *Dansgaard* [1964]).

temperature and relative humidity prevailing at the water vapor source [*Dansgaard*, 1964; *Siegenthaler and Matter*, 1983; *Aristarain et al.*, 1986]. The isotope-temperature relationship might therefore be sensitive to climatic changes. Simple models, however, cannot quantify this sensitivity, since they cannot account for the complexity of the atmospheric circulation and for its interactions with the water cycle. The only numerical tools that allow this type of investigation are the atmospheric general circulation models (AGCMs). They can be used for both present-day and past climatic conditions to investigate the isotope-climate relationship.

The two isotopes, $H_2{}^{18}O$ and HDO, are well correlated on a global scale. The mean oxygen 18-deuterium relationship follows the meteoric water line (MWL) derived by *Craig* [1961] to be $\delta D = 8\ \delta^{18}O + 10$ ‰ (where the isotopic ratios, $\delta^{18}O$ and δD, are defined in per mil as the departures of the $H_2{}^{18}0/H_2{}^{16}O$ and $HDO/H_2{}^{16}O$ mass ratios relative to standard mean ocean water ratios, R_{smow}). If this relationship did not change with climate, we would only be concerned with one isotope species. However, measurements in ice cores have shown that the deuterium excess $d = \delta D - 8\ \delta^{18}O$ may vary by about 5 ‰ in some locations during ice ages [*Jouzel et al.*, 1982]. According to studies with simple model studies, such variations might result from changes in conditions prevailing at the evaporative source regions for the water vapor, e.g. the relative humidity [*Jouzel et al.*, 1982] and the sea surface temperature [*Johnsen et al.*, 1989; *Petit et al.*, 1991]. The simultaneous modeling of both isotopes in an AGCM should also allow an investigation of the deuterium excess-climate relationship.

The first simulations of the atmospheric cycles of the water isotopes were performed on a coarse resolution version of the Laboratoire de Météorologie Dynamique (LMD) AGCM under January conditions [*Joussaume et al.*, 1984]. *Jouzel et al.* [1987*a*] then used the Goddard Institute for Space Studies (GISS) AGCM (with a similar resolution) to simulate global isotope fields over a full seasonal cycle. The two AGCM studies are compared by *Joussaume and Jouzel* [1987]. We present here results obtained with a higher-resolution version of the LMD AGCM. We begin with a description of our modeling. The discussion will then focus on the simulation of the seasonal cycle for the present-day climate, as deduced from simulations of the February and August climates.

To investigate the isotope-climate relationships, we will then examine the sensitivity of the simulated isotope cycles to the present-day-Last Glacial Maximum (LGM) climatic change. The changes in the atmospheric circulation are fully described by *Joussaume* [this issue], referred as part 1 in the present paper, together with the changes of the simulated cycle of desert dust particles. The two parts are, however, mostly independent.

2. Modeling

We present here the main features of the water isotope modeling with the LMD AGCM, and we include a discussion of the basic equations not presented by *Joussaume et al.* [1984]. We have introduced a prognostic equation for each isotope mixing ratio q_i, defined as the mass ratio of water isotopes to the air:

$$\frac{\partial}{\partial t}(rq_i) + \mathrm{div}(rq_i\mathbf{V}) + \frac{\partial}{\partial z}(r_i w) = s_i + r_i + d_i \qquad (1)$$

where ρ is the air density, $\mathbf{V}$ is the horizontal velocity, w is the vertical velocity, and s_i, r_i and d_i are the source, removal and diffusion terms for water isotopes, respectively. The source term corresponds to surface evaporation (or condensation) over oceans and land, and the removal term corresponds to condensation during cloud processes. These two terms involve phase changes and therefore fractionation processes. They are what cause the differentiation of the isotope species during the atmospheric water cycle. The diffusion term corresponds to vertical diffusion within the planetary boundary layer and is parameterized in the same way for all water isotopes.

2.1. *Cloud Processes*

The equation for isotopic equilibrium between the condensed and vapor phases during a condensation process can be written as

$$\frac{q_{ic}}{q_c} = \alpha(T)\frac{q_i}{q} \qquad (2)$$

where q_{ic} and q_c are the isotope and water mixing ratios, respectively, in the condensed phase, and q_i and q are the isotope and water mixing ratios, respectively, in the vapor phase. The fractionation coefficient α is a function of isotope species and the form of the condensed phase (i.e., solid or liquid). This coefficient is always above 1, reflecting the enrichment in heavier isotopes of the condensed phase relative to the vapor phase. The values used in the model and a detailed description of water isotope physics can be found in the work of *Jouzel* [1986].

The hypothesis of complete equilibrium between the condensed and vapor phase is, however, only valid for droplets which have a suitably long residence time. The other extreme hypothesis corresponds to the Rayleigh model, which assumes that isotopic equilibrium occurs only between the vapor and the newly formed fraction of condensate:

$$\frac{\mathrm{d}q_i}{\mathrm{d}q} = \alpha(T)\frac{q_i}{q} \qquad (3)$$

This hypothesis is more suitable for larger drops or for solid formation, for which the time required to reach equilibrium is much longer than the residence time. Integrating this formula between the initial (q_{io},q_o) and final state (q_i,q) of the phase change and assuming α is constant leads to the relationship $q_i = q_{io}(q/q_o)^{\alpha}$.

The Rayleigh model allows a good understanding of the isotope-temperature relationship [*Dansgaard,* 1964]. Applying (3) to a saturated air mass, the change in the isotopic ratio δ_c of the condensed phase between two successive condensations at temperatures T and $T - dT$ is found to be

$$d\delta_c = (1 + \delta_c)\left(\frac{1}{\alpha}\frac{d\alpha}{dT} + (\alpha - 1)\frac{1}{q_s}\frac{\partial q_s}{\partial T}\right) dT \qquad (4)$$

(Note that δ values are related to mixing ratios by the equation $(1 + \delta 10^{-3}) = q_i/(q*R_{smow})$.) The most important contribution to $d\delta_c$ comes from the second term in (4) and leads to $\delta^{18}O$-temperature slopes of about 0.6 for liquid and 1.5 for solid.

In our isotope modeling, we use the Rayleigh model (or "open system" assumption) when solid is formed during condensation, and we use the total equilibrium assumption (or "closed system") when liquid is formed. For the reevaporation of falling drops within and below clouds, we apply the total equilibrium assumption for the liquid phase and assume no fractionation for the solid, i.e., evaporation is assumed to occur at the isotopic ratio of the solid because molecular exchanges with the rest of the solid are very slow.

We allow separate reservoirs for the liquid and solid phases, since the liquid can be formed between -10°C and 0°C under supercooling conditions and since the solid phase only melts above 0°C. We distinguish between nonconvective and convective clouds for the water isotope cycle. In convective clouds, upward motion can allow the liquid phase to exist down to -20°C. In nonconvective clouds, we only keep track of one isotopic reservoir between 0°C and -10°C (the solid one) since the liquid water formed below 0°C has time to freeze before reaching the layer below due to the relatively small size of droplets. Other differences, which concern the treatment of kinetic effects, will be discussed later.

In the LMD AGCM, the nonconvective clouds, which correspond to stratiform clouds, form when the air is conditionally stable and oversaturated. Convection is parameterized using adjustment techniques when the air is conditionally unstable. Two parameterizations are used: the moist adiabatic adjustment method of *Manabe et al.* [1965] when the air is oversaturated, and a cloud parameterization based on the method of *Kuo* [1964] when a convergence of moisture at the top of the boundary layer provides enough moisture to develop a cloud on a fraction of the mesh. However, the adjustment techniques are not at all adequate for tracer modeling as was discussed in a previous paper describing the modeling of the desert dust cycle [*Joussaume,* 1990]. Indeed, the cloud model provides only the final profiles of humidity and temperature, giving no information on the thermodynamic history of air masses inside the cloud. In particular, the respective contributions of convective diffusion and condensation to the change of humidity at each level remain unknown but are required for tracers.

Thus, in order to model convective diffusion, we have introduced an intermediate step of total mixing for the water vapor and the water isotope species. This assumption results in a strong condensation in the higher layers of the clouds and a strong evaporation in the lower layers, thus in part compensating for the strong diffusion associated with the total mixing assumption. However, if this assumption is probably reasonable for the dust particles, it is certainly more critical for the isotopes since fractionation is sensitive to the phase change temperature and the amount of condensed water. In order to weaken this problem, we use an averaged fractionation coefficient to account for upward motion, determined by the average of the coefficients at the local and cloud base temperatures, and we apply the total equilibrium assumption for liquid formation, since this model is symmetrical for both evaporation and condensation, conversely to the Rayleigh model.

2.2. *Surface Fluxes*

To compute the fluxes of water isotopes from the ocean surface, a bulk aerodynamic formula, similar to the one used for the water vapor flux, has been added:

$$s_i = \frac{1}{\Delta z_1}\rho_a C_{Di}\left(1. + |\mathbf{V}_1|\right)\left(q_{is} - q_{ia}\right) \qquad (5)$$

where ρ_a is the surface air density, $\mathbf{V}_1$ is the wind velocity at the first σ level of the model, q_{ia} is the isotope mixing ratio near the surface extrapolated from the two first σ levels, and Δz_1 is the first layer thickness. The drag coefficient C_{Di} is related to the drag coefficient for water vapor C_D through the equation $C_{Di} = C_D\,(1 - k_i)$. The coefficient k_i depends on the molecular diffusivity of each isotope species and accounts for differing efficiencies of the evaporation for different water isotopes. This coefficient is a function of the surface wind speed which is given by *Merlivat and Jouzel* [1979] for oxygen 18 and is multiplied by 0.88 for deuterium. Near the ocean surface, water vapor is in isotopic equilibrium with the ocean, and we therefore compute $q_{is} = q_s*R_{ocean}/\alpha(T_s)$, where α is the isotopic fractionation coefficient at the sea surface temperature T_s. The R_{ocean} coefficient is the mean isotopic content of the ocean and differs for the present-day and LGM climates (section 3). (Note that R_{ocean} for the present-day climate is equal to R_{smow}.)

Over the continents, the exchanges of water molecules are less efficient and the vegetation can introduce fractionation processes leading to either an enrichment or a depletion in heavy isotopes. Therefore, over land, the evaporation of isotope species s_i is computed without fractionation and thus according to the equation $s_i = s*R_g$, where s is the water evaporation and R_g is the isotopic ratio of the ground water reservoir. A prognostic equation of the soil water mass has been added for each isotope species to compute R_g. In the LMD AGCM, a snow reservoir and a one-layer groundwater reservoir of 15 cm maximum water content are considered in the basic hydrologic cycle. For isotopes, a single reservoir that includes both snow and groundwater is used, since no fractionation occurs during snow melting and evaporation. However, this assumption is only valid because we consider perpetual February and August simulations and no full seasonal cycle. Over bare ice, the surface water reservoir is reduced to 1 cm of water in order to average the isotopic ratios of precipitation over a maximum of 10 days even given the low precipitation rates in these regions. For bare sea ice, the isotopic content is controlled by the freezing of seawater and has been set to +3 ‰ and +20 ‰ for oxygen 18 and deuterium, respectively.

When condensation occurs over land or over oceans, the condensed phase is considered to be in isotopic equilibrium with the vapor at the first σ level.

2.3. *Kinetic Effects*

Kinetic effects on isotopic fractionation occur when the change of phase is not at the equilibrium, i.e., when the air is supersaturated or subsaturated. For example, this happens when solid is formed in very cold environments or when large drops evaporate, i.e., when the residence time of the condensate in the air is smaller than the time required to reach equilibrium. Kinetic effects essentially play a role in determining the oxygen 18-deuterium relationship.

From the Rayleigh model (4), we see that the slope of the deuterium-oxygen 18 relationship for the condensed phase is mainly controlled by the ratio $(\alpha_D-1)/(\alpha_{18_O}-1)$ which varies between 8 and 10. The increase in $\alpha-1$ with decreasing temperature is in great part compensated by the decreasing values of the term $(1+\delta_c)$, leading to a quasi-constant δD-$\delta^{18}O$ slope of about 8. For processes at equilibrium, the fractionation is thus about 8 times more efficient for deuterium than for oxygen 18. However, kinetic effects tend to be about the same for both isotope species, due to close molecular diffusivities, and they can therefore modify the δD-$\delta^{18}O$ slope.

Kinetic effects can be parameterized with an effective fractionation coefficient α_e. During condensation (evaporation), the slower molecular exchanges of the heavier isotopes induce a decreased (increased) enrichment of the condensed phase, corresponding to $\alpha_e < \alpha$ ($\alpha_e > \alpha$).

For condensation, the effective fractionation coefficient can be written as a function of the relative humidity S and the ratio a of molecular diffusivities [*Jouzel and Merlivat*, 1984]:

$$\alpha_e = \alpha \left(\frac{aS}{a + \alpha (S-1)} \right) \tag{6}$$

The parameterization of the supersaturation ratio S is based on results obtained from simple models in order to improve the agreement with observations at high latitudes [*Jouzel and Merlivat*, 1984]: $S = \max(1.20, 0.99\text{-}0.006\ t)$, where t is the temperature in degrees Celsius. This relationship slightly differs from the one used in the previous experiments described by *Joussaume et al.* [1984]. Kinetic effects associated with solid condensate formation have only been included for nonconvective clouds, since they can occur at higher latitudes and thus in cooler environments. Nevertheless, the parameter S is the only one that is fitted on empirical data of the δD-$\delta^{18}O$ relationship, whereas all the other parameters used in our water isotope modeling result from laboratory or theoretical data.

The formula (6) is also applied during the reevaporation of falling rain under the base of convective clouds. In this situation, in agreement with *Stewart* [1975], we use $a = (D_i/D)^{0.58}$, where D_i and D are the diffusivities of the isotope and water, respectively. For the subsaturation S, we assume an average value between 1 and the initial value of S in the grid box.

The introduction of a kinetic effect tends to decrease the δD-$\delta^{18}O$ slope of precipitation in both cases. For the formation of solid at high latitudes, the slope is then closer to 8, and for the reevaporation, the slope decreases to values around 4.

Kinetic effects have also been included in the parameterization of the surface fluxes over oceans through the use of C_{Di}. These processes are important as they determine the value of the deuterium excess of near-surface water vapor over source regions. Indeed, from simple model studies, using (5) and assuming the same isotopic content for the vapor flux and the near-surface vapor [*Merlivat and Jouzel*, 1979], the deuterium excess in the near-surface vapor is seen to be a decreasing function of both the sea surface temperature and the relative humidity. The value of 10 ‰ is obtained from simple models for a mean temperature of 25°C and a mean relative humidity of 80%, which are reasonable values over oceanic tropical regions.

2.4. *Transport*

The simplest way to transport the isotope species is to use the same numerical scheme as the one used in the basic water cycle. However, two conditions must be met to ensure a reasonable treatment of water isotopes: water isotopes and water must be transported as consistently as possible, and the occurrence of negative mixing ratios must be avoided since they lead to dramatic inconsistencies in isotopic ratios. The first condition is ensured by applying the numerical scheme to isotopic ratios, which are the relevant variables for water isotopes. To ensure the second condition, the numerical scheme used for vertical transport of water vapor was modified from the standard version of the LMD AGCM [*Joussaume et al.*, 1984].

For horizontal transport, we use an upstream scheme for both water and its isotopes. This scheme perfectly satisfies the two above mentioned conditions. However, it is a first-order scheme that is highly diffusive [*Joussaume*, 1990]. This last defect might affect our isotopic results, as seen from sensitivity experiments performed with the GISS model [*Jouzel et al.*, 1991]. This scheme is not used to determine the vertical transport of water, since it would lead to an excessive amount of condensation in the upper troposphere. A second-order scheme is instead used that is based on the harmonic averaging of water and on the arithmetic averaging of the isotopic ratios between two grid points [*Joussaume et al.*, 1984].

3. NUMERICAL EXPERIMENTS

Simulations of perpetual February and perpetual August climate under both present-day and LGM conditions have been performed; these four experiments are described in part 1. The initial atmospheric content of water isotopes was set everywhere to -80 ‰ for $\delta^{18}O$ and -600 ‰ for δD in each experiment, since these values are well below the observed ones. The initial ground isotopic ratios R_g were determined from the surface temperature using the climatological $\delta^{18}O$-temperature relationship obtained by *Dansgaard* [1964] and the MWL for the δD-$\delta^{18}O$ relationship.

The following analyses concern fields averaged over the last 60 days of 100-day simulations. A spin-up time of 40 days is indeed sufficient to reach equilibrium isotopic ratios in the global mean atmospheric, precipitation and evaporation fields (Figure 2). However, the global mean ground isotopic ratio does not completely reach its equilibrium after 40 days (Figure 2). Although we set R_g to an initial state near the equilibrium, the time to recover from the low isotopic ratios of the first 10 days is indeed longer than 40 days. The analyses, however, essentially remain valid as this deficiency only applies to regions of low soil water content, which are poor sources of water vapor for the atmosphere.

The use of a 60-day average may also bias the isotope results, since a 60-day average cannot account for all the low frequencies of the atmospheric circulation. This bias results from the high computer requirements of tracer models.

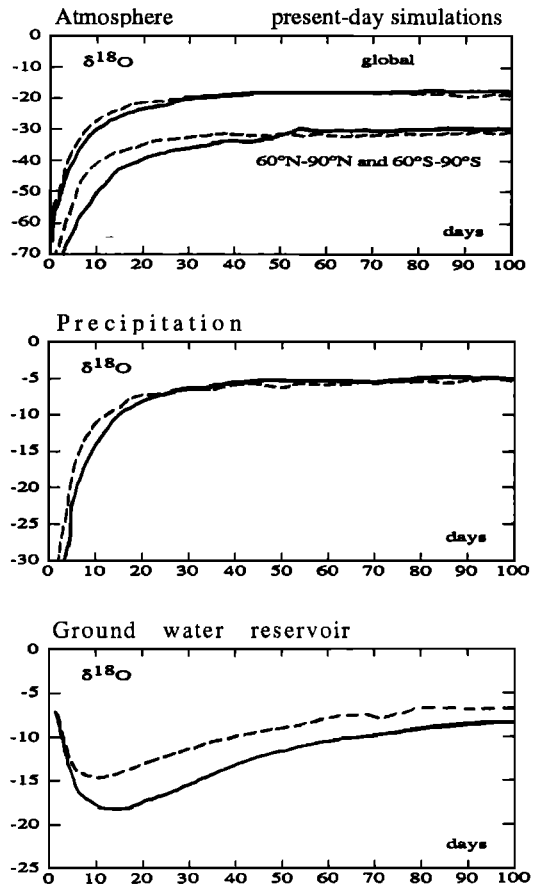

Fig. 2. From top to bottom, time evolution of atmospheric $\delta^{18}O$ content, both global and high-latitude (> 60°) averages, time evolution of $\delta^{18}O$ in precipitation and time evolution of the groundwater reservoir. Results are for the present-day February (dotted line) and August (solid line) simulations.

Nevertheless, our present results must be considered as a first approach, of more meteorological than climatological relevance, that can help diagnose some of the main aspects of the water isotope-climate relationship but cannot bring an extensive study of the problem.

The only change introduced in the isotope formulations between the simulations of the present-day and LGM climates is in the prescribed value of the ocean's isotopic ratio, R_{ocean}. For the present-day climate, R_{ocean} for $H_2{}^{18}O$ is set to 0 ‰ and for the LGM to 1.6 ‰ [*Duplessy*, 1981]. The shift in R_{ocean} results from the storage of isotope poor waters in the LGM ice sheets. The shift, however, might be slightly overestimated according to the more recent estimate of 1.1 ‰ for the LGM oxygen 18 value given by *Labeyrie et al.* [1987]. The change in deuterium is then deduced from the change in oxygen 18, using the MWL relationship [*Craig*, 1961] in the ocean water mass balance for present-day and LGM conditions. The change in deuterium is thus set to 12.8 ‰, i.e., 8 times the change in oxygen 18.

4. THE PRESENT-DAY CLIMATE

We focus the analyses on the simulated isotopic contents of precipitation and on their relations to meteorological parameters. We will discuss both the annual mean fields, as derived from the averages of February and August results, and their seasonal contrast. The predicted results will be compared to data obtained by the International Atomic Energy Agency (IAEA) network [*IAEA*, 1981] combined with data for Greenland and Antarctica [*Jouzel et al.*, 1987*a*].

The simulated field of annual mean oxygen 18 content in precipitation (Figure 3) is characterized by rich isotopic ratios in tropical regions and decreasing ratios toward high latitudes. We discuss separately the tropical and extratropical regions, since isotope behavior in these regions is dominated by different meteorological parameters.

4.1. *Tropical Regions and the Amount Effect*

In tropical regions, the spatial field of $\delta^{18}O$ values in precipitation is characterized by well-defined patterns of rich (> -2 ‰) and poor (< -4 ‰) ratios. Although similar patterns are also shown in observations (Figure 3), the observed patterns do not exactly correspond with the simulated ones, e.g., over the southern Pacific Ocean, the Indian Ocean and Africa.

In tropical regions, $\delta^{18}O$ values are poorly correlated with temperature but are better correlated with precipitation amounts, with high ratios corresponding to low precipitation rates and vice versa. This correlation with precipitation, called the "amount effect" by *Dansgaard* [1964], largely controls the tropical $\delta^{18}O$ field, as indicated by a comparison of the February fields of $\delta^{18}O$ (Figure 4) and precipitation (part 1 or *Joussaume* [1990]). The simulated mean $\delta^{18}O$-precipitation relationship for regions with surface air temperatures above 15°C has a slope of -0 62 ‰/100 mm d^{-1}, approximately 30% stronger than the observed slope (-0.48 ‰/100 mm d^{-1} [*Jouzel et al.*, 1987*a*]). In the model, the basic mechanism leading to the amount effect seems to be a strong isotopic enrichment of falling precipitation during reevaporation under the cloud base, as is indicated by low associated deuterium excess values (section 4.4). The other mechanism proposed by *Dansgaard* [1964] assesses that the vapor forming the rain is more depleted in heavy isotopes in regions of high precipitation rates, but this is not corroborated by the simulated isotopic content of the vapor [*Joussaume*, 1989].

The predicted correlation between $\delta^{18}O$ and precipitation is relatively poor (correlation coefficient of -0.3). Nevertheless, some of the discrepancies between the observed and simulated $\delta^{18}O$ charts can be explained by deficiencies in the simulated precipitation field (part 1 or *Joussaume* [1990]). The low isotopic ratios in the southern Pacific in February (Figure 4) result from the overestimated South Pacific Convergence Zone (part 1), whereas excessively rich ratios are simulated over Indonesia where the model underestimates the winter monsoon precipitation. In February, the simulated minimum isotopic ratios over southern Africa are displaced toward the continent, following the simulated precipitation field. The discrepancies between model results and observations are larger in August than in February, leading to the main deficiencies of the simulated seasonal contrast (Figure 4). The model isotopic ratios in the African and Indian monsoon rains are too rich, perhaps due partly to the underestimation of the simulated precipitation over these regions. Some other discrepancies, e.g., the poor isotopic ratios over Arabia in August, cannot be explained by the amount effect and will be discussed later (section 4.3).

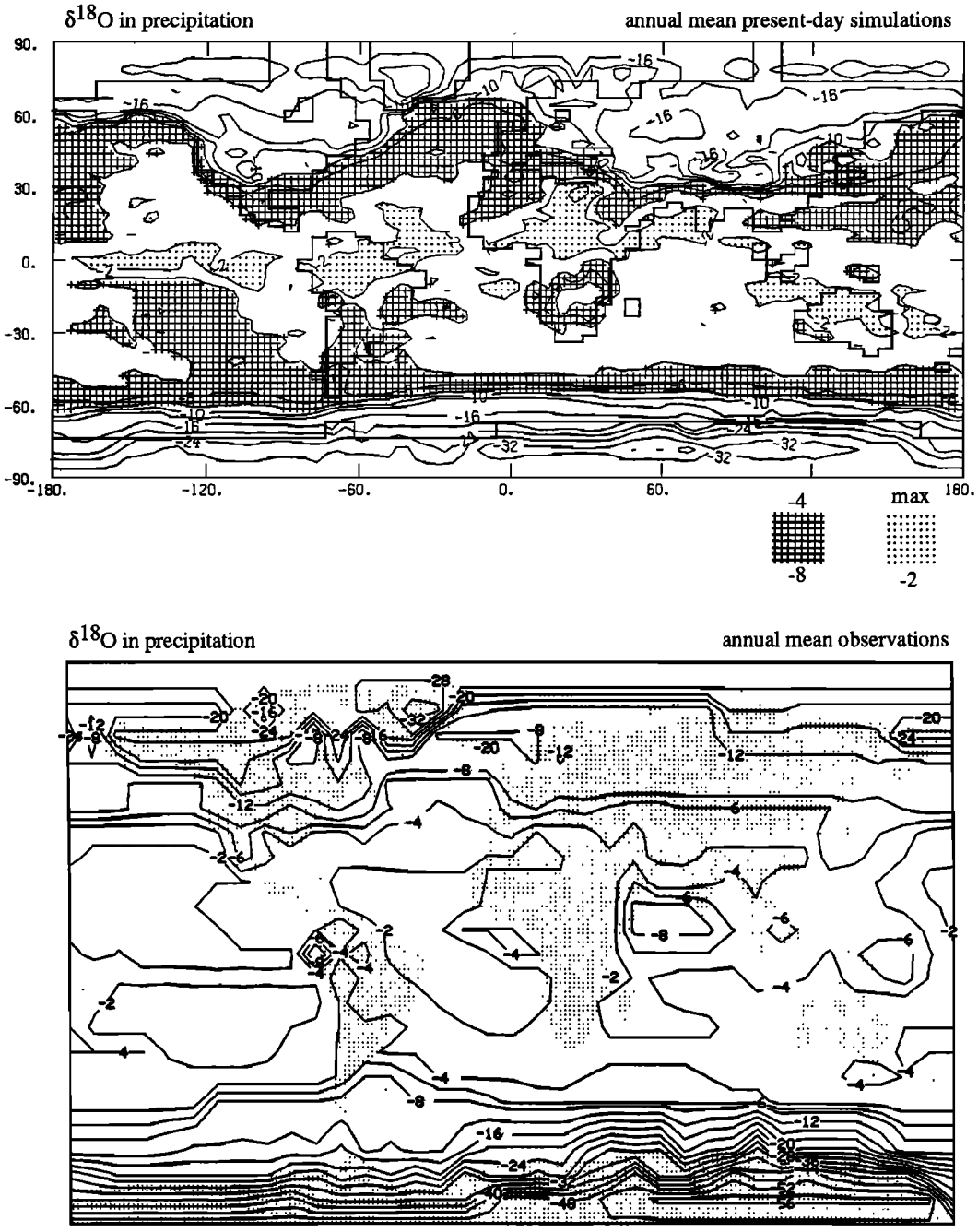

Fig. 3. Annual mean $\delta^{18}O$ in precipitation for the present-day climate: comparison between the (top) simulation results and (bottom) observations. Isolines are provided at every 2 ‰ (4 ‰) above (below) -12 ‰ for the simulations and above -8 ‰ for the observations (adapted from *Jouzel et al.* [1987*a*]).

4.2. *The Extratropical Regions and the $\delta^{18}O$-Temperature Relationship*

In the northern hemisphere, the annual mean simulated isotopic ratios are in good agreement with observations (Figure 3), particularly over Europe. The simulated minima of -24 ‰ and -20 ‰ over Greenland and northern America, respectively, are, however, slightly underestimated by about 4 ‰, although the seasonal contrast (as represented by August $\delta^{18}O$ values minus February $\delta^{18}O$ values in Figure 4) is reasonably well represented. It is noteworthy that our model produces a realistic seasonal contrast over Greenland with $\delta^{18}O$ values around 8 ‰, whereas the GISS model did not obtain any seasonal dependency in isotopic ratios there despite a reasonable seasonal cycle of temperature [*Jouzel et al.*, 1987*a*]. The comparison is more limited over Siberia due to lack of data; the straight isocontours over Siberia shown in the observational field result from linear interpolation applied along latitudinal circles (Figure 3).

In the southern hemisphere, the simulated meridional gradient of $\delta^{18}O$ is largely underestimated. Over East Antarctica, the simulated ratios of -32 ‰ are much larger than the observed values of -52 ‰. However, the isotopic ratios in this region are mainly controlled by the surface air temperature field (Figure 5), and the strong discrepancy over Antarctica

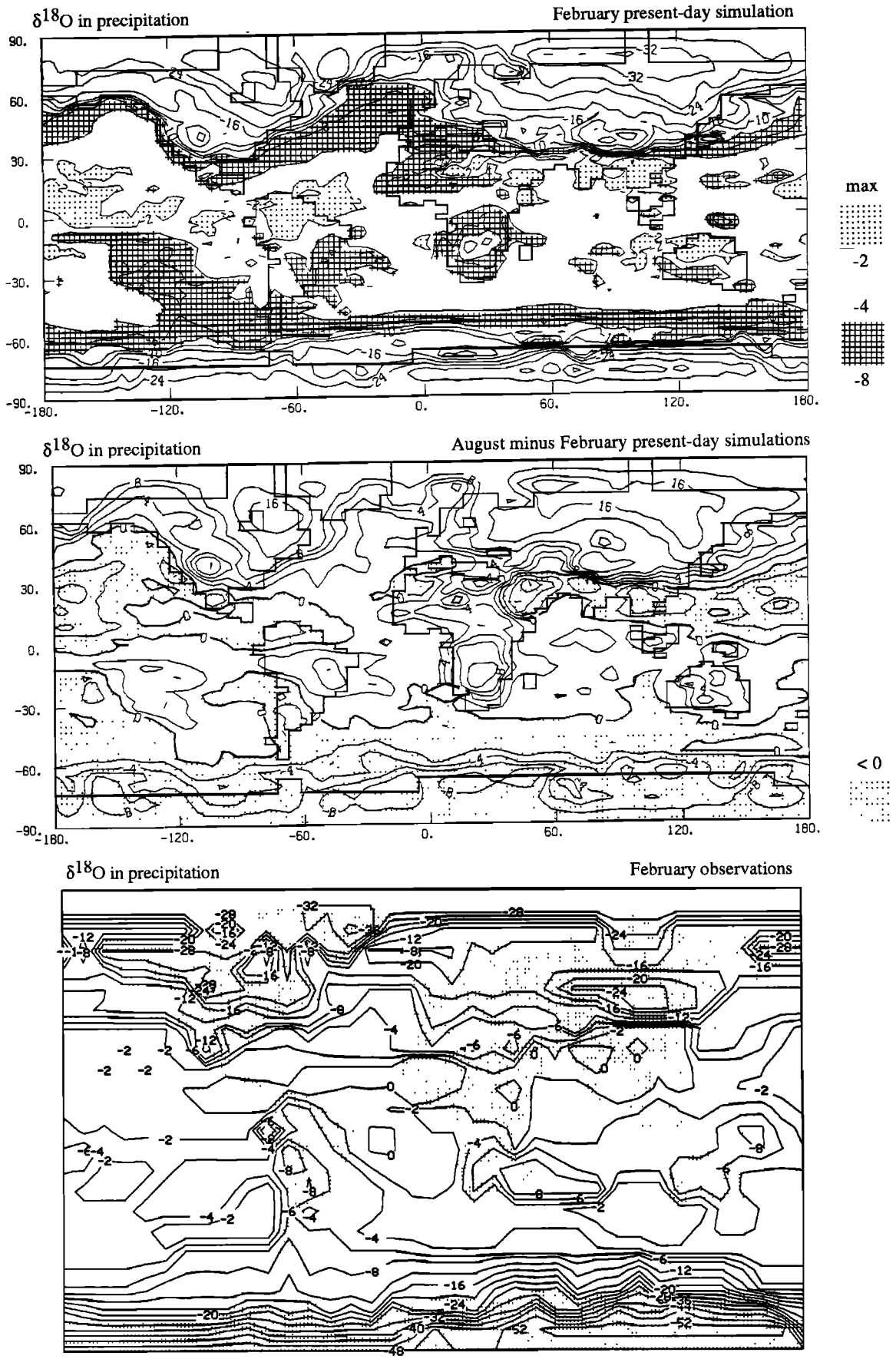

Fig. 4. (Top) February and (bottom) August minus February mean $\delta^{18}O$ in precipitation for the present-day climate: comparison between the simulation results and observations (courtesy of R. Suozzo). For the August minus February fields, isolines are at every 2 ‰.The simulated difference map has been smoothed using a five-element filter (with weights of one half for the grid point and one eighth for its four nearest neighbors) and uses a 4 ‰ isoline increment above 8 ‰.

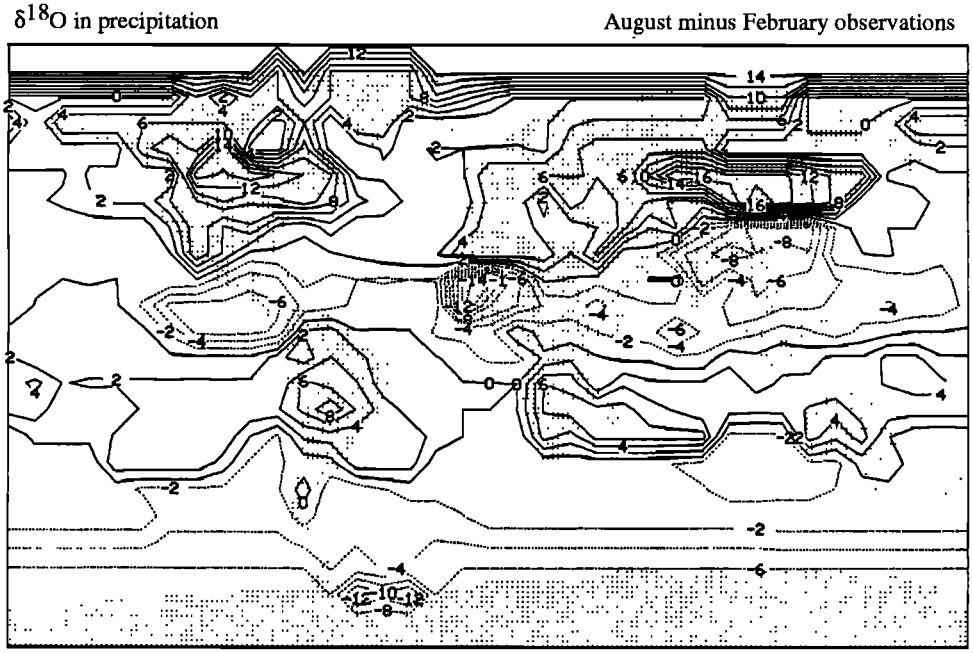

Fig. 4. (continued)

might result from the overestimation of the simulated surface air temperatures there [*Joussaume*, 1990], which are warmer by 15° to 20°C compared to observed values [*Taljaard et al.*, 1969]. The simulated snow accumulation is also stronger than the observed one over these regions (Table 5). A test of the model's isotopic cycle that avoids the model's deficiencies in temperature prediction is a comparison of the simulated $\delta^{18}O$-temperature relationship with the observed relationship.

The predicted oxygen 18-surface air temperature relationship exhibits an overall pattern in very good agreement with observations (Figure 5). For temperatures below 15°C, the simulated and observed slopes are similar, with values of 0.64 and 0.57, respectively (Table 1). Both the predicted and observed slopes decrease above 15°C with respective values of 0.16 and 0.06. A smaller slope for warmer temperatures is indeed expected due to the lower fractionation coefficient for the liquid-vapor transition (as compared to that for the solid-vapor phase change) and due to the mixing of both temperature and mixing ratios during convection [*Jouzel*, 1986].

However, in the model, the change of slope more clearly appears around 0°C rather than 15°C as in the observations and the correlation remains relatively high above 0°C (Table 2). The simulated results are characterized by relatively rich ratios around 0°C for precipitation over the southern hemisphere oceanic regions; the discrepancy might therefore result from the lack of observations in this region. The GISS isotopic model [*Jouzel et al.*, 1987*a*], however, agrees with observations more closely. The richer values produced by the LMD model might then be favored by the turbulent vertical mixing within the planetary boundary layer, which is included in the LMD AGCM but not in the GISS AGCM. In any case, sensitivity experiments would be required to diagnose the source of this particular feature.

The overall $\delta^{18}O$-temperature relationship is similar for February and August (Figure 6). A higher dispersion of the isotopic ratios is, however, simulated in August above 0°C, largely as a result of northern hemisphere precipitation (Figure 6). As seen from the regional averages (Table 3), the slopes decrease in the northern hemisphere summer, particularly over continents with values around 0.20. Although this feature is in general corroborated by observations (Table 3), the model disagrees with observations over North America.

The simulated slopes increase toward higher latitudes. The model predicts annual mean slopes of 1.33 and 0.92 over Greenland and Antarctica, respectively. These two values are stronger than the corresponding observed values of 0.63 and 0.78 (Table 3). However, over Antarctica, the model does not reproduce well the near-surface temperature inversion. Our results are indeed in better agreement with the slope of 1.1 estimated from the condensation temperature [*Jouzel and Merlivat*, 1984] than they are with the slope of 0.78 associated with the surface temperature.

4.3. *Relationships With Other Meteorological Parameters*

The observed and predicted $\delta^{18}O$-temperature values are scattered around the mean relationship in a similar way (Figure 5). We can use the model results to investigate the origin of this scattering. We display for February and August the difference between the local $\delta^{18}O$ values and the isotopic content $\delta^{18}O_T$ deduced from the annual mean $\delta^{18}O$-temperature relationship at the local surface air temperature T_a (Figure 7, Table 2).

The effect of topography is evident, with lower ratios over the Rockies and the Himalayas. This altitude effect was indeed mentioned by *Dansgaard* [1964]. It probably results from a higher altitude of condensation, where the isotopic ratios in vapor are lower.

The shift from the mean temperature dependency, $\delta^{18}O$ minus $\delta^{18}O_T$, exhibits other well-defined patterns. In the following, we try to determine if these patterns mainly reflect the transport of water vapor from the oceans. It is indeed possible that a higher depletion in heavy isotopes occurs for

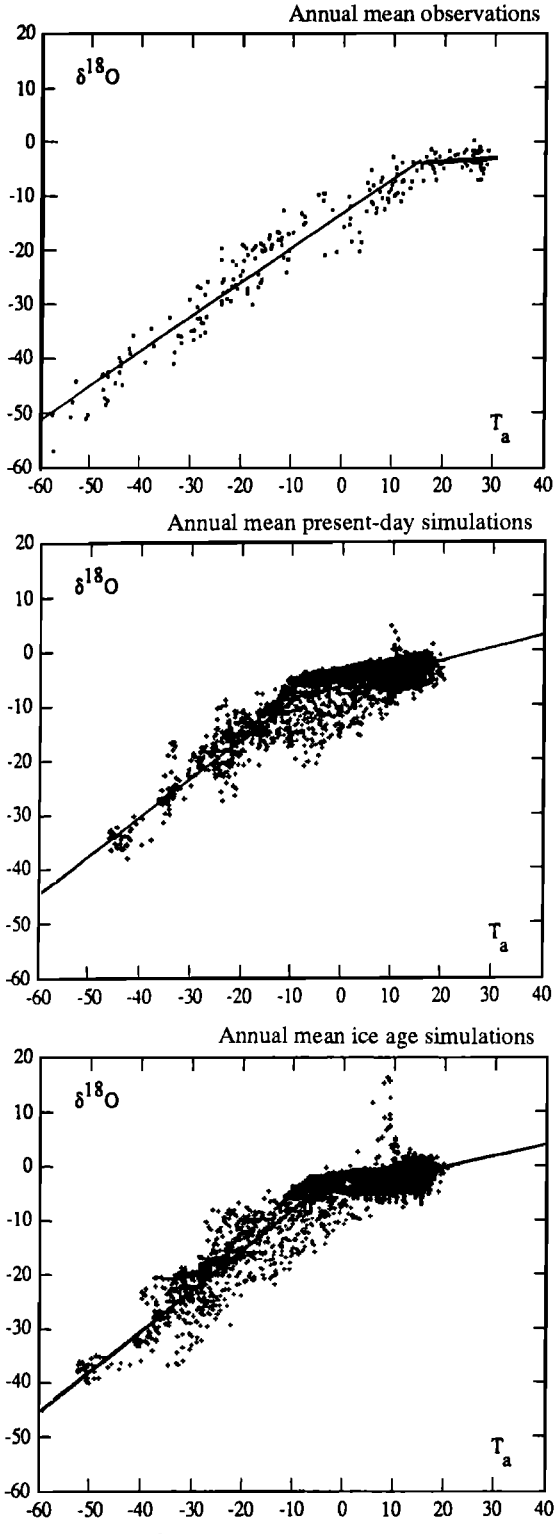

Fig. 5. Annual $\delta^{18}O$ in precipitation versus annual surface air temperature T_a from observations (adapted from *Jouzel et al.* [1987*a*]), and from the present-day and ice age simulations. In the simulations, T_a is extrapolated linearly from the two first model σ layers. Each graph contains two linear least squares fits, one for temperatures below a certain cutoff temperature and the other for the higher temperatures. This cutoff temperature is 15°C for the observations (see Table 1) and 0°C for the simulations (see Table 2).

water vapor farther from the vapor source due to the fact that it has experienced more condensation processes.

In agreement with this proposed mechanism, the shift is positive over the oceans, which are the main source of water vapor, and negative over most continental areas. The largest decreases are toward the interior of continents. The depletion is particularly intense in August over the northern hemisphere continents, and might result from an increased influence of local evaporation at the ground isotopic ratios, which are essentially governed by the mean isotopic content of precipitation (lower than the oceanic mean ratio). These intense negative values thus probably reflect the poor oceanic influence inside the continents during the summer season, a phenomenon confirmed by numerical experiments tracing the origin of water vapor in July [*Joussaume et al.*, 1986]. The influence of local evaporation on the isotopic ratios was also emphasized by *Rozanski et al.* [1982].

We can compare the $\delta^{18}O$ minus $\delta^{18}O_T$ shift to the mean low-level atmospheric circulation, i.e., to the sea level pressure fields (Figure 7). Over Europe, an east-west gradient of the $\delta^{18}O$ minus $\delta^{18}O_T$ shift is generated for both seasons. This pattern seems to be associated with the transport of water vapor from the Atlantic by the westerlies as is inferred by the coincidence between the $\delta^{18}O$ minus $\delta^{18}O_T$ shift and the sea level pressure patterns in August. In February, the lower values of the shift over Europe also follow the stationary cyclonic circulation located over central Europe, which tends to inhibit oceanic influence. Also, in February, positive values of the shift are found over northwestern America following the transport of water vapor from the northern Pacific by the westerlies associated with the continental anticyclonic circulation.

The impact of transport is clearly visible over Arabia in August, where low values follow the simulated northerlies. However, in this case, the simulated low oxygen 18 content of precipitation is not corroborated by observations (Figure 4). This discrepancy probably emphasizes model deficiencies: the overestimation of the northerlies and the high diffusivity along streamlines resulting from the numerical scheme used for transport (section 2).

Very few analyses based on observations have been performed to study the impact of other meteorological parameters. Nevertheless, *Siegenthaler and Matter* [1983] have shown that the isotopic content of precipitation over western Europe does exhibit a stronger depletion toward the interior of the continent even at constant temperature, thus corroborating our simulated results.

Simple isotope parcel models display a sensitivity of the $\delta^{18}O$-temperature relationship to other meteorological parameters as well. In particular, they show a dependency on the air temperature prevailing over the water vapor source region [*Aristarain et al.*, 1986]: the isotope-temperature relationship is displaced toward richer isotopic contents for lower source temperatures, since a smaller difference between the source and condensation temperatures induces fewer condensation processes. This mechanism might explain the positive shifts that are obtained in our AGCM studies at high latitudes, both in February over the northeastern Atlantic Ocean and in August near Antarctica.

4.4. *The δD-$\delta^{18}O$ Relationship*

The predicted oxygen 18 and deuterium contents of precipitation are very well correlated, as indicated by the 0.99 value of the correlation coefficient in Figure 8. The annual mean relationship produced by the model compares well with IAEA data (Figure 8, Table 4) and with the meteoric water line defined by *Craig* [1961]. To better analyze this relationship we use the deuterium excess $d = \delta D - 8\,\delta^{18}O$ (Figure 9).

TABLE 1. Comparison Between the Predicted and Observed Present-Day $\delta^{18}O$-Surface Air Temperature T_a Relationships, for Annual Méan, February and August Conditions

	Predicted Present-day		Observations	
	Relationship	r	Relationship	r
		Annual Mean		
$T_a > 15°C$	$0.16\,T_a - 7.0$	0.31	slope 0.06	0.15
$T_a < 15°C$	$0.57\,T_a - 11.4$	0.88	slope 0.64	0.96
		February		
$T_a > 15°C$	$0.10\,T_a - 5.4$	0.22	$-0.10\,T_a - 0.75$	-0.11
$T_a < 15°C$	$0.69\,T_a - 11.0$	0.94	$0.55\,T_a - 11.9$	0.85
		August		
$T_a > 15°C$	$0.02\,T_a - 3.5$	0.03	$0.29\,T_a - 11.0$	0.38
$T_a < 15°C$	$0.52\,T_a - 11.1$	0.86	$0.44\,T_a - 12.2$	0.63

Separate relationships are computed for T_a above and below 15°C. The correlation coefficients r are included.

TABLE 2. Comparison Between The Predicted Present-day and Ice Age $\delta^{18}O$-Surface Air Temperature Ta Relationships, for Annual Mean, February and August Conditions

	Predicted Present-day		Predicted Ice Age	
	Relationship	r	Relationship	r
		Annual Mean		
$Ta > 0°C$	$0.23\,Ta - 8.8$	0.60	$0.22\,Ta - 6.4$	0.57
$Ta < 0°C$	$0.71\,Ta - 9.7$	0.91	$0.74\,Ta - 8.2$	0.86
		February		
$Ta > 0°C$	$0.17\,Ta - 7.0$	0.61	$0.15\,Ta - 4.5$	0.38
$Ta < 0°C$	$0.71\,Ta - 10.9$	0.88	$0.64\,Ta - 11.0$	0.88
		August		
$Ta > 0°C$	$0.18\,Ta - 7.6$	0.41	$0.19\,Ta - 5.8$	0.43
$Ta < 0°C$	$0.59\,Ta - 10.0$	0.87	$0.44\,Ta - 12.0$	0.79

Separate relationships are computed for T_a above and below 15°C. The correlation coefficients r are included.

Over the oceans, the model predicts d values that lie between 8 and 10 ‰ in tropical regions and that decrease down to 4 ‰ in higher latitudes. These results are well corroborated by observations (Figure 9).

The simulated d values over continents are lower than those over the oceans, with continental values generally below 4 ‰. Many continental areas even experience negative deuterium excess in the model. The low deuterium excesses are generally found over dry regions. They are generated by the kinetic fractionation processes occurring during the reevaporation of falling drops below the cloud base. A lowering of the δD-$\delta^{18}O$ slopes is indeed related to the low d values and is visible in Figure 8. Over Africa, the simulated February δD-$\delta^{18}O$ slope is 6, and is well corroborated by *IAEA* [1981] data [*Joussaume,* 1989]. Slope values as low as 4 have even been observed [*Yurtsever and Gat,* 1981]. Low d values are also obtained in observations but with most values around 0 to 4 ‰ (Figure 9). Although d values as low as -18 ‰ or -20 ‰ are observed in February in Bamako (Mali) or in California [*IAEA,* 1981], the model seems to overestimate the intensity and extent of the low values. The model sensitivity to the kinetic effect over dry regions is clearly demonstrated by the relationship between δD and the relative humidity over continents shown in Figure 10. It is not clear why this sensitivity was less pronounced in the first simulations of January presented by *Joussaume et al.* [1984]. The process of reevaporation below the cloud base deserves an improved parameterization.

The model underestimates the deuterium excess over Antarctica with simulated values of 2 to 4 ‰ compared to observed values of 8 to 14 ‰. The simulated values are more comparable to coastal values [*Petit et al., 1991*]. According to these observations, the deuterium excess increases with decreasing temperature. The model deficiency might then result from our overestimation of the surface air temperatures over Antarctica. Note that the GISS model, which generates better temperatures in this area, also generates better deuterium excess there [*Jouzel et al.,* 1987*a*]. Our results might also be sensitive to the supersaturation function used in the model, although for low temperatures the maximum value of 1.20 is reached (section 2.3). Over Greenland, the simulated results are in good agreement with observations, with a mean simulated value of 7 ‰ compared to an average observed value of 8 ‰ [*Johnsen et al.,* 1989].

The low deuterium excess values over coastal areas in Antarctica correspond to the general decreasing trend of

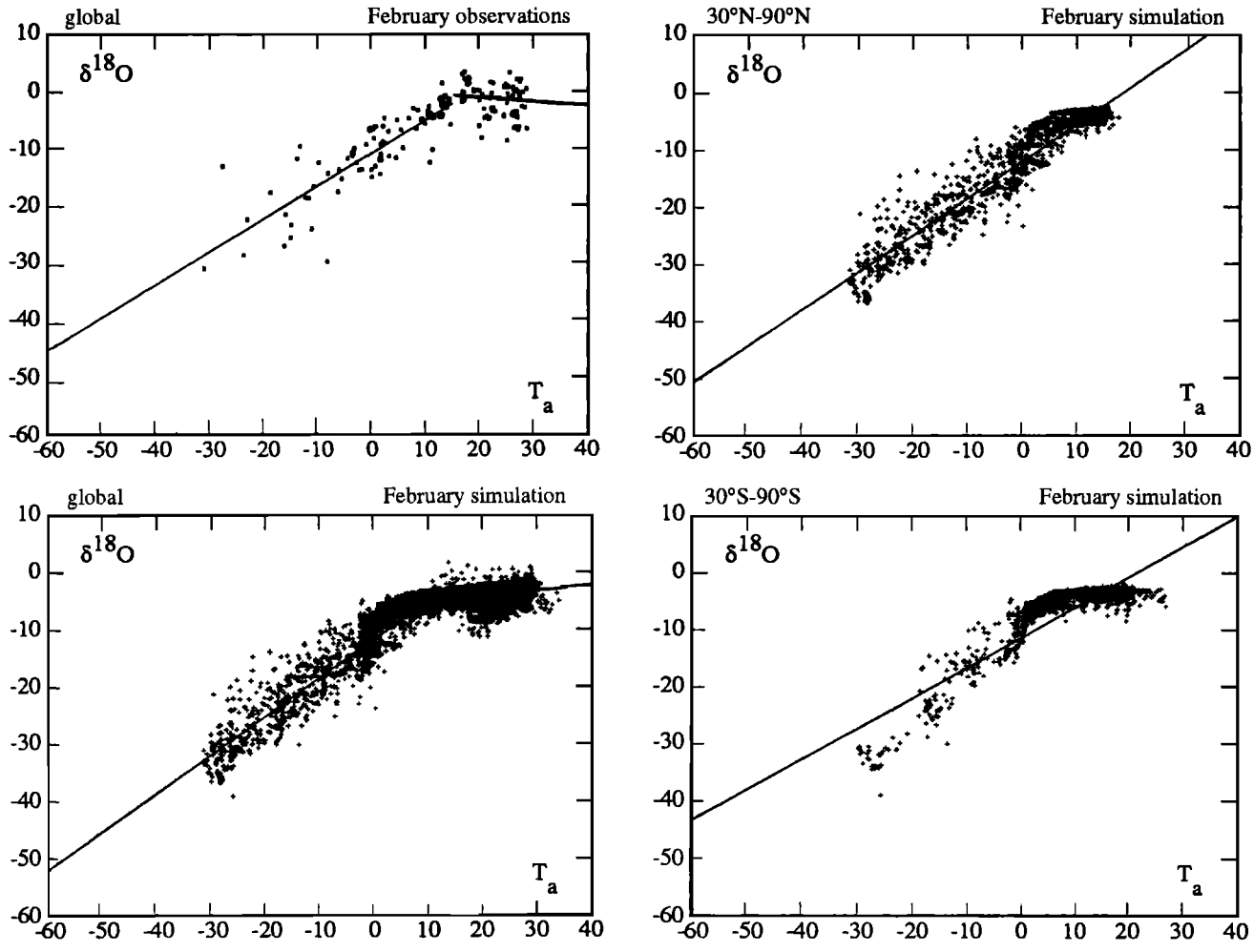

Fig. 6a. February $\delta^{18}O$ in precipitation versus surface air temperature T_a for the present-day simulation and observations (courtesy of R. Suozzo). The associated least squares fit lines are separated at 15°C for data on a global scale (see Table 1). For the simulations, the northern and southern hemisphere extratropical $\delta^{18}O$-T_a relationships are also displayed for each season. Their respective least squares fit lines are $0.65T_a - 11.9$ (correlation coefficient $r = 0.94$) and $0.54T_a - 10.9$ ($r = 0.89$).

deuterium excess toward high latitudes. According to simple isotopic models [*Jouzel et al.*, 1982; *Johnsen et al.*, 1989], lower deuterium excess can result from both higher relative humidity $S = q/q_S$ and lower sea surface temperatures T_S at the water vapor source regions. We thus analyze the simulated relationships between the surface air deuterium excess over the oceans and S and between this deuterium excess and T_S (Figure 11). The deuterium excess clearly correlates better with T_S than with S. This result supports the interpretation that low deuterium excess values over Antarctica during the LGM are related to changes of sea surface temperature over the source regions rather than to changes in relative humidity [*Johnsen et al.*, 1989].

5. The Ice Age Climate

In the following, we discuss the changes in the isotopic content of precipitation generated in a simulation of the LGM climate and compare them to available isotopic paleoclimatic data. We also analyze the simulated changes in δD-$\delta^{18}O$ and $\delta^{18}O$-temperature relationships.

5.1. *The $\delta^{18}O$ Content of Precipitation*

In the simulation of the LGM, the annual mean oxygen 18 content of precipitation (Figure 12) is 0 to 2 ‰ richer in the tropics than it is in the present-day climate. This increase mainly reflects the prescribed increase in the mean oceanic isotope content from 0 to 1.6 ‰ for the LGM. Over the Sahara, the simulated increase is stronger, with values up to 8 ‰ due to an increased aridity; the mean $\delta^{18}O$-precipitation relationship is not modified during the LGM.

Outside of tropical regions, the oxygen 18 content of precipitation is lower during the LGM. In the northern hemisphere, the lowest values are located over the Laurentide and Fennoscandian ice sheets and reach -12 ‰. In the southern hemisphere, they are located over sea ice and reach -8 ‰. These changes are in great part controlled by changes in surface air temperature (Figure 13).

5.2. *Comparison With Paleoclimatic Data*

Ice core data. Paleoclimatic data of the isotopic content of precipitation can be obtained by measuring the isotopic

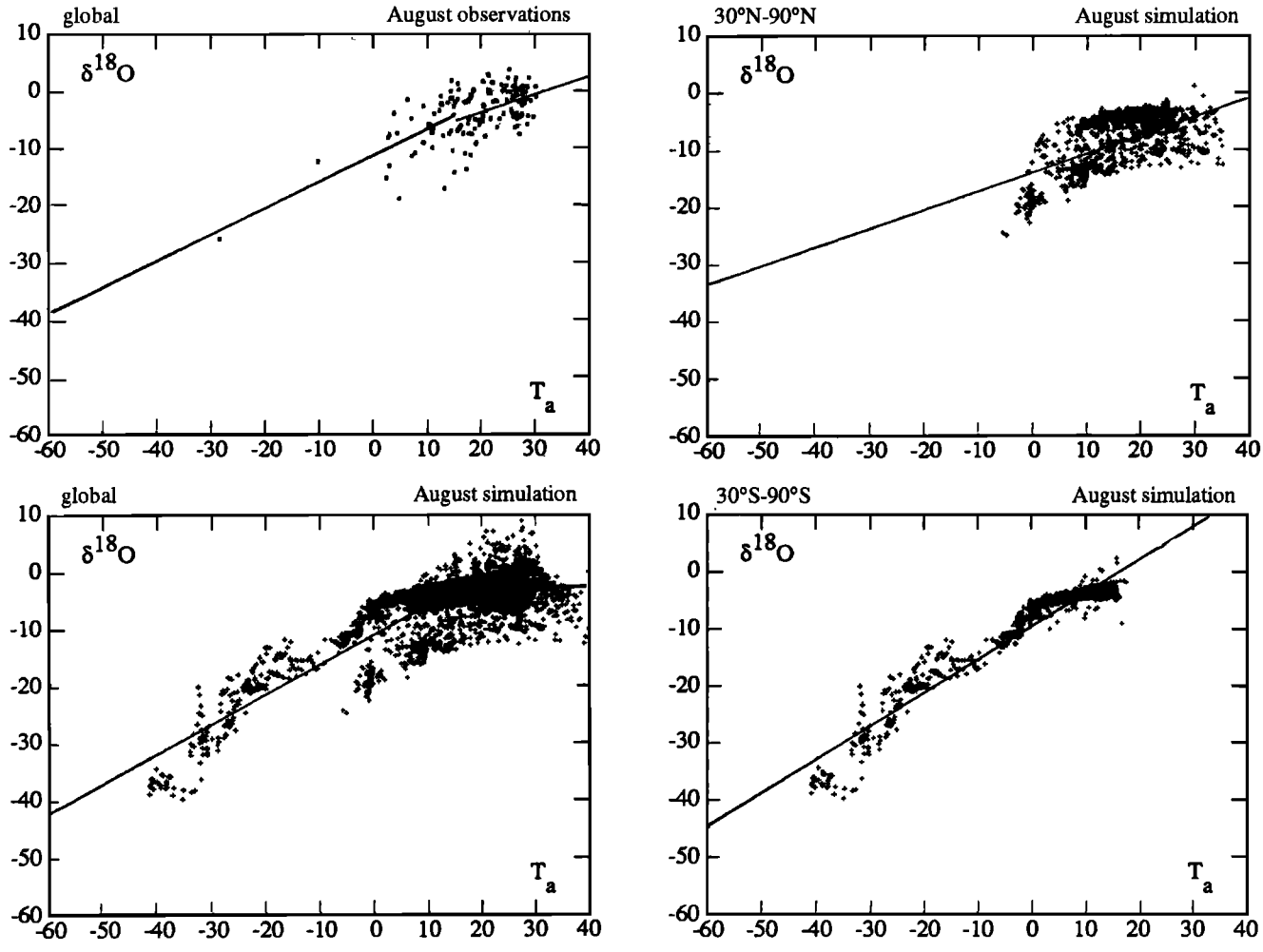

Fig. 6b. Same as Figure 6a but for August. The northern and southern hemisphere least squares fit lines are $0.33T_a - 13.7$ ($r = 0.61$) and $0.59T_a - 9.1$ ($r = 0.96$).

contents of ice cores drilled in Antarctica and Greenland. Data have been obtained in East Antarctica at Dôme C [*Lorius et al.*, 1979] and Vostok [*Lorius et al.*, 1985] stations, in West Antarctica at Byrd station [*Epstein et al.*, 1970; *Johnsen et al.*, 1972], and in Greenland at Camp Century and Dye 3 stations [*Dansgaard et al.*, 1969; *Johnsen et al.*, 1972; *Dansgaard et al.*, 1982].

In East Antarctica, all the paleoclimatic data indicate a $\delta^{18}O$ lowering of -5 ‰ during the LGM, and this is confirmed by data from a new core in Dôme B (77°S, 90°E) (J. Jouzel, private communication, 1988). In the model, the average changes over East Antarctica are -6 ‰ near the coast and -3 ‰ in the interior (Table 5). The simulated changes are thus reasonable for Dôme C, which is located between the two model latitudes, but are underestimated by 2 ‰ for Vostok, even though, as will be discussed later, the simulated temperature change for both stations is -8°C. In West Antarctica, the model's decrease in $\delta^{18}O$ is too weak with a value of -0.7 ‰; the observed value at Byrd is -7 ‰. The simulated change in surface air temperature is also weak in this area, especially considering that topography was set 1000 m higher during the simulated LGM (Table 5). Over Greenland, the simulated reductions of $\delta^{18}O$ are of -10 ‰, in between the reductions measured in the Camp Century and Dye 3 cores (Table 5).

Other sources of paleoclimatic data. Outside the ice caps, paleoclimatic data can be obtained from isotopic measurements in groundwater [*Bath*, 1983], in speleothems and their fluid inclusions [*Schwarcz and Yonge*, 1983], and in ancient wood cellulose [*Yapp and Epstein*, 1977]. The latter two sources give access to δD rather than $\delta^{18}O$. The simulated changes in δD (Figure 12) mainly follow the simulated changes in $\delta^{18}O$ (Figure 12), since the mean δD-$\delta^{18}O$ relationship remains globally unchanged (section 5.3).

Over most of Europe (around 50°N and between 10°W and 30°E), groundwaters give a change in δD of the order of -12 ‰ [*Rozanski*, 1985]. The model results are in good agreement with this change, with simulated changes between 0 and -2 ‰ for $\delta^{18}O$. In England, however, the model estimates the decrease of $\delta^{18}O$ to be -4 ‰, a larger decrease than the observed -1.2 ‰ [*Bath*, 1983]. The simulated positive change in $\delta^{18}O$ in eastern Europe is not corroborated by paleoclimatic data and is probably associated with the unrealistic increase of temperatures simulated in February (part 1).

In southern North America, the model simulates changes in δD values of around 20 ‰, in very good agreement with the δD change estimated from the wood cellulose by *Yapp and Epstein* [1977]. This change is stronger than the change of the mean oceanic isotope content, and a study of seasonal

TABLE 3. Slopes and Correlation Coefficients of the $\delta^{18}O$-T_a Relationships Over Various Regions, for the Observed, Predicted Present-Day and Predicted Ice Age Results

	Observed		Predicted Present-Day		Predicted Ice Age	
	Slope	r	Slope	r	Slope	r
			February			
Continents > 60°N	0.47	0.83	0.69	0.81	0.64	0.89
Oceans > 60°N	0.52	0.91	0.62	0.95	0.59	0.94
North America	0.69	0.93	0.59	0.93	0.78	0.97
Eurasia	0.60	0.91	0.57	0.93	0.57	0.90
Oceans 30°S-30°N	0.16	0.26	0.12	0.27	0.09	0.22
South America	-0.19	-0.39	0.20	0.64	0.25	0.65
Africa	0.75	0.61	0.13	0.25	0.03	0.03
Oceans < 30°S	0.41	0.84	0.35	0.79	0.56	0.94
			August			
Continents > 60°N	0.26	0.57	0.49	0.57	0.53	0.84
Oceans > 60°N	0.41	0.68	0.45	0.77	0.56	0.84
North America	0.68	0.73	0.24	0.68	0.68	0.92
Eurasia	0.23	0.54	0.20	0.44	0.33	0.67
Oceans 30°S-30°N	0.11	0.20	-0.06	-0.14	-0.11	-0.24
South America	0.29	0.74	0.35	0.84	0.40	0.81
Africa	-0.24	-0.57	-0.20	-0.34	-0.16	-0.24
Oceans < 30°S	0.53	0.97	0.49	0.96	0.53	0.97
			Annual Mean			
Antarctica	0.78	0.94	0.92	0.89	0.80	0.94
Greenland	0.63	0.99	1.33	0.73	1.31	0.54

variations suggests that it is not temperature dependent. It can be associated with changes in the water vapor source regions: the North Pacific, for example, exhibits strong simulated evaporation fluxes during the LGM (part 1). However, other paleoclimatic data do not corroborate the δD increase: estimates from fluid inclusions in speleothems give a δD mean change of -12 ‰ over North America [*Schwarcz and Yonge*, 1983] and groundwater in New Mexico give a -25 ‰ change [*Phillips et al.*, 1986]. The diversity of the isotopic paleoclimatic data demonstrates how difficult the interpretation of these measurements can be and limits their use in the validation of the model results.

5.3 *Changes in the δD-δ¹⁸O Relationship and the Deuterium Excess*

The predicted mean δD-$\delta^{18}O$ relationship remains practically unchanged during the LGM climate, as seen in Figure 8. The only visible change is an increased occurrence of rich isotopic ratios associated with much lower deuterium excess. According to the changes in deuterium excess in Figure 12, the lower d values are simulated in tropical regions and result from an increased aridity, especially over the Sahara-Arabia deserts. Measurements of the deuterium excess in groundwater of North Africa do not corroborate the simulated trend; they indicate a decrease of 5 ‰ [*Sonntag et al.*, 1979], which is smaller than the simulated one of -8 to -12 ‰. These groundwater, however, were formed around 20 kyr B.P. during a wet period and might not represent the Last Glacial Maximum period.

Above the continents, changes in deuterium excess are essentially controlled by changes in humidity. For example, in Europe, the increased values of d (by 4 ‰) are associated with increased precipitation, particularly in August. These results are, however, not corroborated by observations, which show no change in European d values for the LGM [*Rozanski*, 1985]. This discrepancy may be related to an incorrect simulation of LGM precipitation in Europe (part 1) and to the overestimated model sensitivity of deuterium excess to humidity (section 4.4). Above the Laurentide ice sheet, the model predicts an increase in d, perhaps resulting from the formation of snow during the LGM, with snow formation preventing kinetic fractionation during reevaporation under the cloud base.

At Dôme C in Antarctica, ice core data indicate a 4 ‰ decrease in the deuterium excess during the LGM [*Jouzel et al.*, 1982]. The decrease is smaller in the AGCM, being of the order of 1 to 2.5 ‰. Moreover, the spatial variability is high, with simulated differences varying from -7 to +3 ‰. Paleoclimatic data in Greenland exhibit small changes in d [*Johnsen et al.*, 1989], whereas the model results give a mean increase of 3 ‰.

The observed decrease in deuterium excess in Antarctica has been interpreted as being related to an increase in the relative humidity over the oceanic source regions [*Jouzel et al.*, 1982] combined with a 2°-3°C lowering of the source regions' temperatures [*Johnsen et al.*, 1989; *Petit et al.*, 1991]. As mentioned in section 4.4, our simulated results tend to confirm this second mechanism, especially since no change in the relative humidity over the southern hemisphere oceans was simulated. However, since the model is not able to simulate the observed change in deuterium excess for the LGM, no conclusions concerning this point can be made from the present study.

5.4 *The δ¹⁸O-Temperature Relationship*

The mean $\delta^{18}O$-surface air temperature relationship is very similar for both climates (Figure 5), as is also reflected in the associated mean slopes (Table 2). The mean regression lines reflect, for temperatures lower than 0°C, a slight shift between the LGM and modern isotopic ratios which is close to the 1.6 ‰ shift of the oceanic ratio. The shift is slightly higher in tropical regions (2.4 ‰), reflecting a further enrichment due to an increased aridity.

The changes in the $\delta^{18}O$-temperature relationship are more important on regional and seasonal bases (Table 3). The slopes and correlation coefficients tend to be larger for the LGM, particularly over the northern hemisphere continents in August. The most important change is a twofold increase of the slope over North America where the Laurentide ice sheet maintains low temperatures even during the summer season.

6. DISCUSSION

The main objective in the interpretation of isotopic paleoclimatic data is to relate the time variations of $\delta^{18}O$, expressed as $\Delta\delta^{18}O$ (differences between past and present-day $\delta^{18}O$ values), to the time variations of the surface air temperature (ΔT_a) at each measurement location. Since such temporal $\delta^{18}O$-T_a relationships are not known, paleoclimatic reconstructions based on isotopic data apply the relationships obtained from the measured present-day spatial distributions of both fields [*Jouzel et al.*, 1987*b*]. Replacing a local time variation by a spatial variation is, however, only valid if the spatial $\delta^{18}O$-temperature relationship does not vary with time. We can compare the approaches based on the temporal and

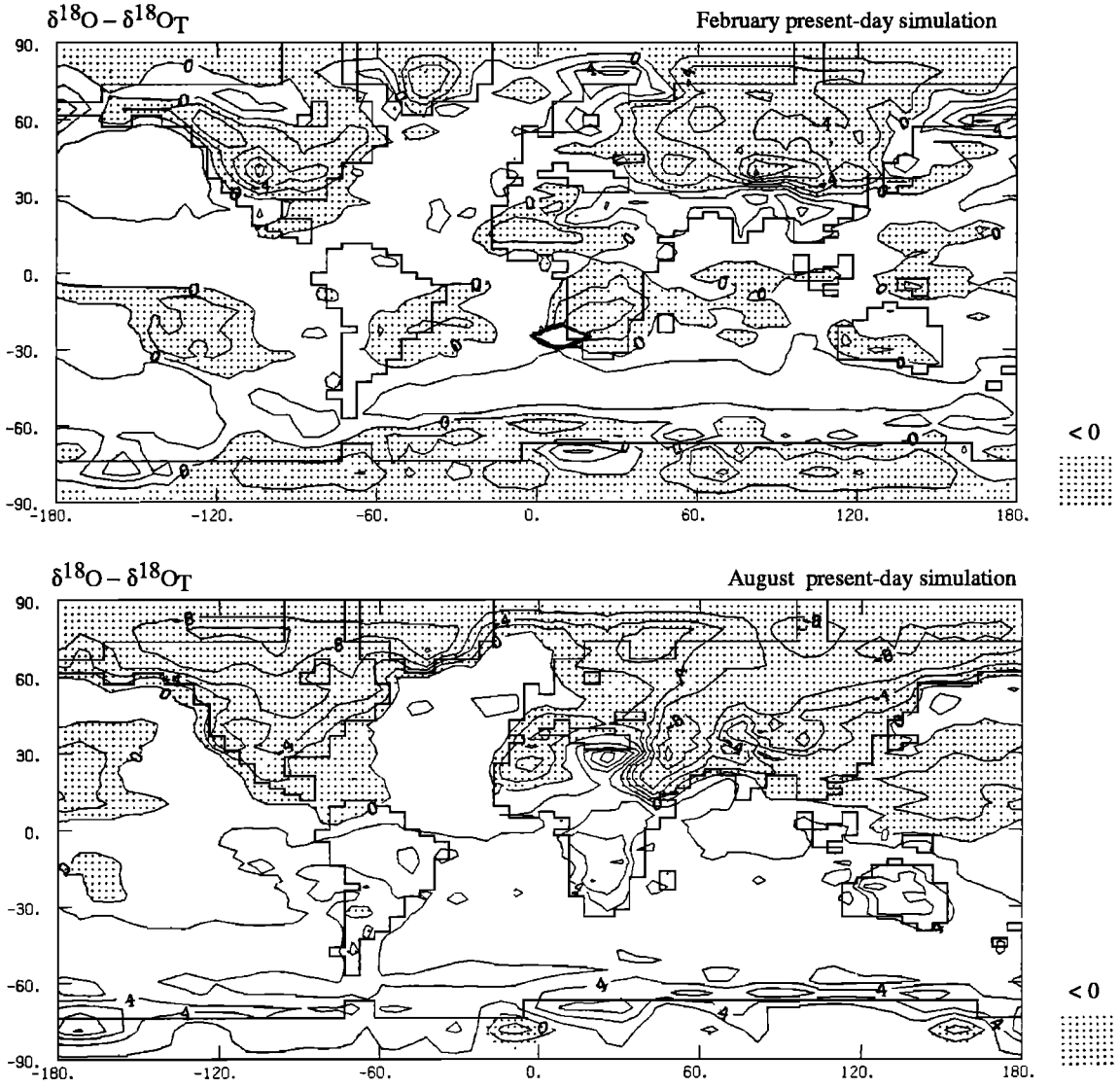

Fig. 7a. The $\delta^{18}O$ shift from the annual mean temperature relationship $\delta^{18}O_T$ ($0.23T_a - 8.8$ ($T_a > 2°C$) and $0.71T_a - 9.7$ ($T_a < 2°C$)) for the simulated February and August precipitation fields of the present-day climate (see text). The temperature domains are separated at 2°C rather than at 0°C to ensure the continuity between the two linear least squares fits (Table 2). The field has been smoothed following the procedure used in Figure 4 and isolines are drawn at every 2 ‰.

spatial relationships through our simulations of present-day and LGM climates.

We consider the simulated results for Greenland and Antarctica. We compute the temporal slope:

$$(\Delta\delta^{18}O - 1.6\ ‰)/\Delta T_a$$

using the simulated time variations of $\delta^{18}O$ and T_a, and compensating for the change in the ocean's isotopic ratio during the LGM. The spatial variability of $\Delta\delta^{18}O$ is relatively high from one grid point to the next, rather more than that of ΔT_a. This feature might be enhanced by our relatively short experiments. We, therefore, average the $\Delta\delta^{18}O$ and ΔT_a values over the regions defined in Table 5 before computing the temporal slopes. In Greenland, the temporal $\delta^{18}O$-T_a slopes are 1.0 for the southern latitudes and 1.6 at 78°N. These values are well represented by the spatial $\delta^{18}O$-T_a slope of 1.3 obtained for the present-day climate in Greenland (Table 3). Over East Antarctica (80°E to 130°E), the temporal slopes are 0.6 and 1.0 at 78°S and 70°S, respectively, which also compare well with the spatial $\delta^{18}O$-T_a slope of 0.9 over Antarctica (Table 3). This fairly good agreement for both regions probably results from the small changes simulated between the present-day and LGM spatial $\delta^{18}O$-temperature relationships (Table 3). Neverthel-ess, the shifts simulated between the temporal and spatial $\delta^{18}O$-T_a slopes can give us an estimate of the error associated with the methodology used in isotopic paleoclimatology. Indeed, from the above mentioned values for Greenland and Antarctica, using spatial slopes rather than temporal slopes induces a relative error on the estimated temperatures of the order of 20 to 30%.

Another way to compare the approaches based on the temporal and spatial relationships through our simulated results is to apply the method used in isotopic paleoclimatology directly to the model output. We first obtain an estimated change in $\delta^{18}O$ (LGM minus present-day), labeled $\Delta\delta^{18}O_T$, from the change in surface air temperature ΔT_a, using the mean $\Delta\delta^{18}O$-T_a relationship,

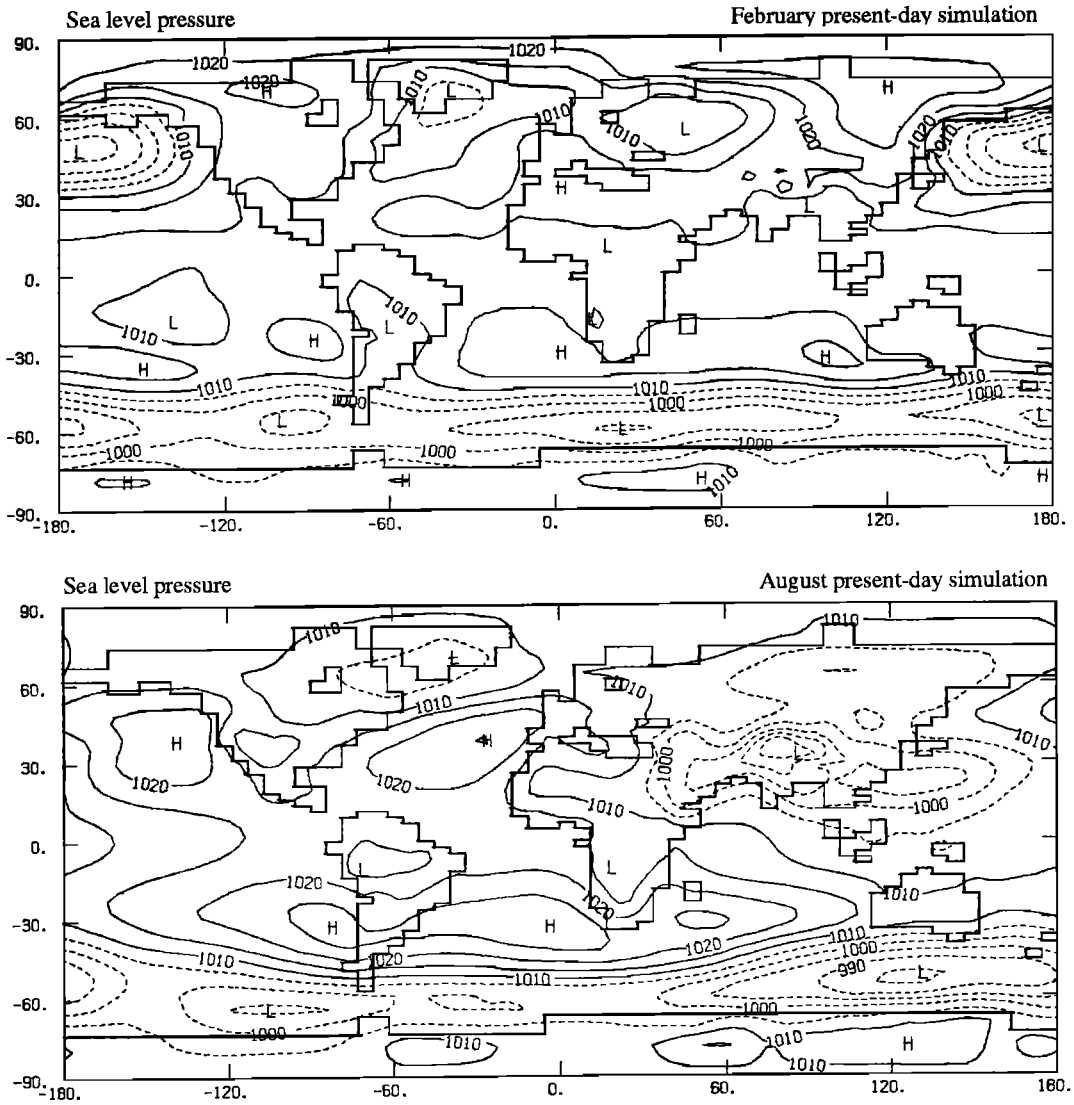

Fig. 7b. February and August sea level pressure fields simulated for the present-day climate. Isolines are at every 5 hPa and are dashed for pressures below 1005 hPa.

$$\Delta\delta^{18}O_T = 0.70\,\Delta T_a + 1.6 \quad (7)$$

which is based on the present-day $\delta^{18}O$-T_a relationship below 0°C (Table 2) and takes into account the change in the ocean's isotopic ratio. It is in good agreement with the relationships used in paleoclimatology for Antarctica (slope of 0.75) and Greenland (slope of 0.69). With (7) we neglect the slope change occurring at 0°C and thus restrict our discussion to regions with surface air temperatures lower than 0°C. Taking $\Delta\delta^{18}O$ to be the actual simulated change in $\delta^{18}O$, we compute the shift $E = \Delta\delta^{18}O - \Delta\delta^{18}O_T$ (Figure 13). The shift E is also a measure of the error made when estimating the actual change in the surface air temperature (ΔT_a) from the change in isotopic ratios (ΔT_e), since $E = 0.70\,(\Delta T_e - \Delta T_a)$. Negative values of E correspond to an overestimation of the cooling, with a shift of -2 ‰ being associated with an overestimated cooling of 3°C.

The simulated shift E displays well-defined patterns with values of several per mil units. North America displays the highest shifts and thus appears to be the worst area in which to use the isotopic ratios for estimating paleotemperatures. These high shifts are related to the strong change in the $\delta^{18}O$-T_a slope in North America between the two climates (Table 3). However, this simulated feature might not be realistic since the simulated slope over North America disagrees with observations during the summer season. Over Greenland, the change in $\delta^{18}O$ is relatively stronger than the one inferred from the temperature change but this is due to a mean $\delta^{18}O$-T_a slope of 1.3 for both climates there (Table 3) which is higher than the slope of 0.70 used to calculate E. This feature suggests that regional $\delta^{18}O$-T_a relationships should be used in paleoclimatic reconstructions rather than globally averaged ones. In East Antarctica, the shift is negative along the coast and positive toward the interior, defining patterns which are not explained by the higher local slope of 0.9 obtained for each climate (Table 3).

Other factors can indeed help determine the patterns of E. As previously discussed, the atmospheric circulation and its effects on the origin of precipitating water are one such factor. To study such a factor, we consider how the $\delta^{18}O$ shift from the mean temperature dependency, i.e., $\delta^{18}O$ minus $\delta^{18}O_T$ (section 4.3), is modified between the simulated present-day (Figure 7) and LGM (Figure 14) February climates. Over Europe, for

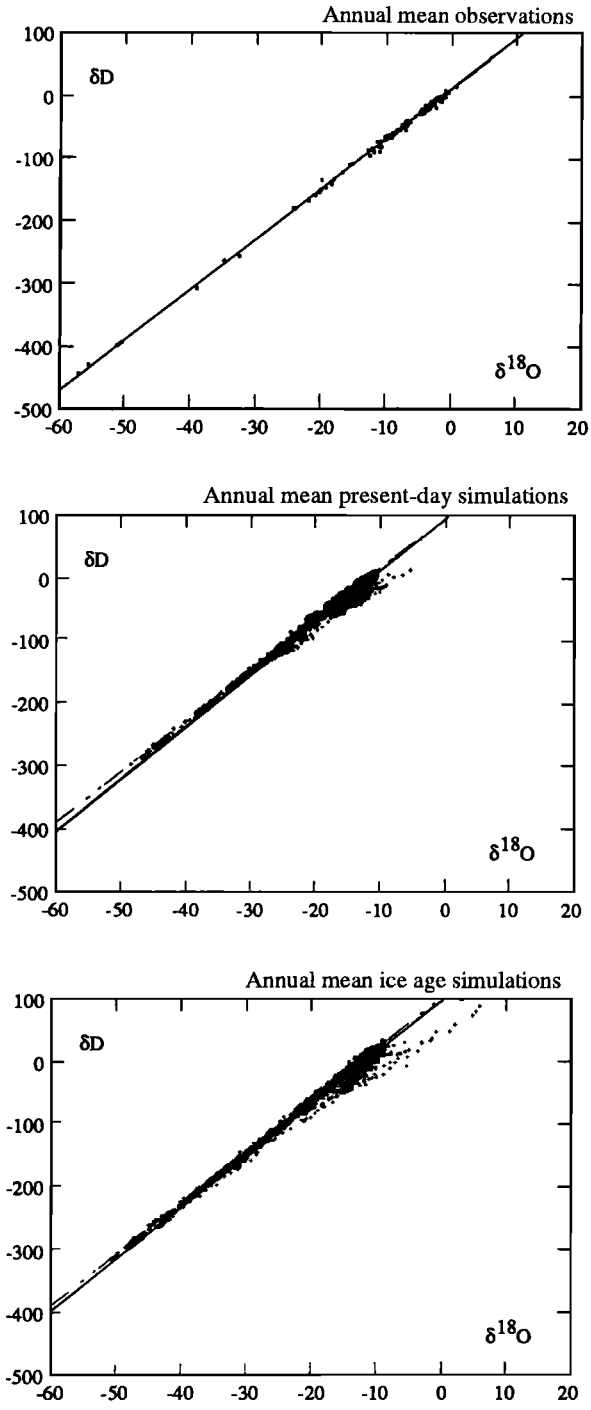

Fig. 8. Annual $\delta^{18}O$ in precipitation versus annual δD in precipitation for observations (adapted from *Jouzel et al.* [1987*a*]) and for the present-day and ice age simulations. The graphs contain the associated linear least squares fits (solid lines) (Table 4) and the meteoric water line (dotted line).

TABLE 4. The Observed and Predicted Present-Day δD-$\delta^{18}O$ Relationships and the Predicted Ice Age Relationship for Annual Mean Precipitation

	Relationship	r
Observed	$\delta D = 7.97\ \delta^{18}O + 8.60$	1.0
Predicted Present-Day	$\delta D = 8.21\ \delta^{18}O + 6.62$	0.99
Predicted Ice Age	$\delta D = 8.08\ \delta^{18}O + 4.95$	0.99

example, the positive $\delta^{18}O$ minus $\delta^{18}O_T$ values in the LGM simulation no longer extend over the northeastern Atlantic Ocean, as in the present-day climate, but penetrate inside western Europe. This change follows the changes in the storm tracks as seen from the patterns of the low pressures in Figures 7 and 14 (also discussed in part 1). Further east in Europe, the positive $\delta^{18}O$ minus $\delta^{18}O_T$ values in the LGM simulation are associated with a transport from tropical regions following the anticyclonic circulation located over the eastern Mediterranean Sea. In Antarctica, the shifts are more negative in the LGM simulation than in the present-day simulation which may result from the equatorward expansion of the sea ice during the LGM, inducing a further depletion in heavy isotopes associated with an increased distance to the water vapor source (Figure 14). In East Antarctica, a tongue of less depleted ratios is simulated in the LGM. This feature is associated with a northeasterly transport of water vapor in this area (Figure 14), favoring richer ratios in the interior rather than on the coast (Table 5).

In addition, changes in the seasonal distribution of precipitation can affect E values (Figure 13). Inside East Antarctica, the strong increase in summer LGM precipitation (part 1) weights the annual average isotopic ratios toward the summer values, thus amplifying the simulation of rich ratios in the interior of the continent (Table 5). This feature reflects a limitation of our study which does not deal with a complete seasonal cycle.

Our simulated isotopic results can also be model dependent. To examine their robustness, we compare them to those of analogous 3-year GISS AGCM simulations of present-day and LGM climates (J. Jouzel et al., unpublished data, 1992). The GISS isotopic model [*Jouzel et al.*, 1987*a*] is very similar to the one we use, except that the GISS model employs a coarser horizontal grid, a higher-order numerical scheme for isotope transport, and different parameterizations for physical processes. Some preliminary results of the GISS LGM simulations were described by *Joussaume and Jouzel* [1987], together with comparisons of the two AGCMs concerning the simulated present-day isotopic cycles.

In agreement with the LMD model, the GISS model suggests that the changes in the global $\delta^{18}O$-T_a and δD-$\delta^{18}O$ relationships between the present-day and LGM climates are very small (Table 6). However, the LMD and GISS model results can differ on a regional basis. For example, the LMD model suggests a very poor reconstruction of paleotemperatures using paleo-isotopic ratios over North America, while the GISS model suggests the opposite. Over Greenland, the changes in $\delta^{18}O$ are weaker in the GISS AGCM (Table 7), leading to a mean temporal $\delta^{18}O$-T_a slope of 0.5 rather than the slopes of 1 to 1.6 obtained from the LMD model. The temporal and spatial $\delta^{18}O$-T_a slopes are, however, similar to each other in both the LMD and GISS models. Over East Antarctica, the temporal $\delta^{18}O$-T_a slope decreases from the coast to the interior in the LMD model, but it increases in the GISS model from 1 at 74°S to 2 at 82°S. Both models exhibit a high spatial variabil-ity in $\Delta\delta^{18}O$, despite a low spatial variability in ΔT_a, showing that the variability simulated by the LMD model in this area does not entirely result from our short numerical experiments.

The origins of these discrepancies are difficult to determine. One important source might be the different transport schemes used by the two AGCMs, especially at high latitudes, which are far from the water vapor source regions. The high sensitivity

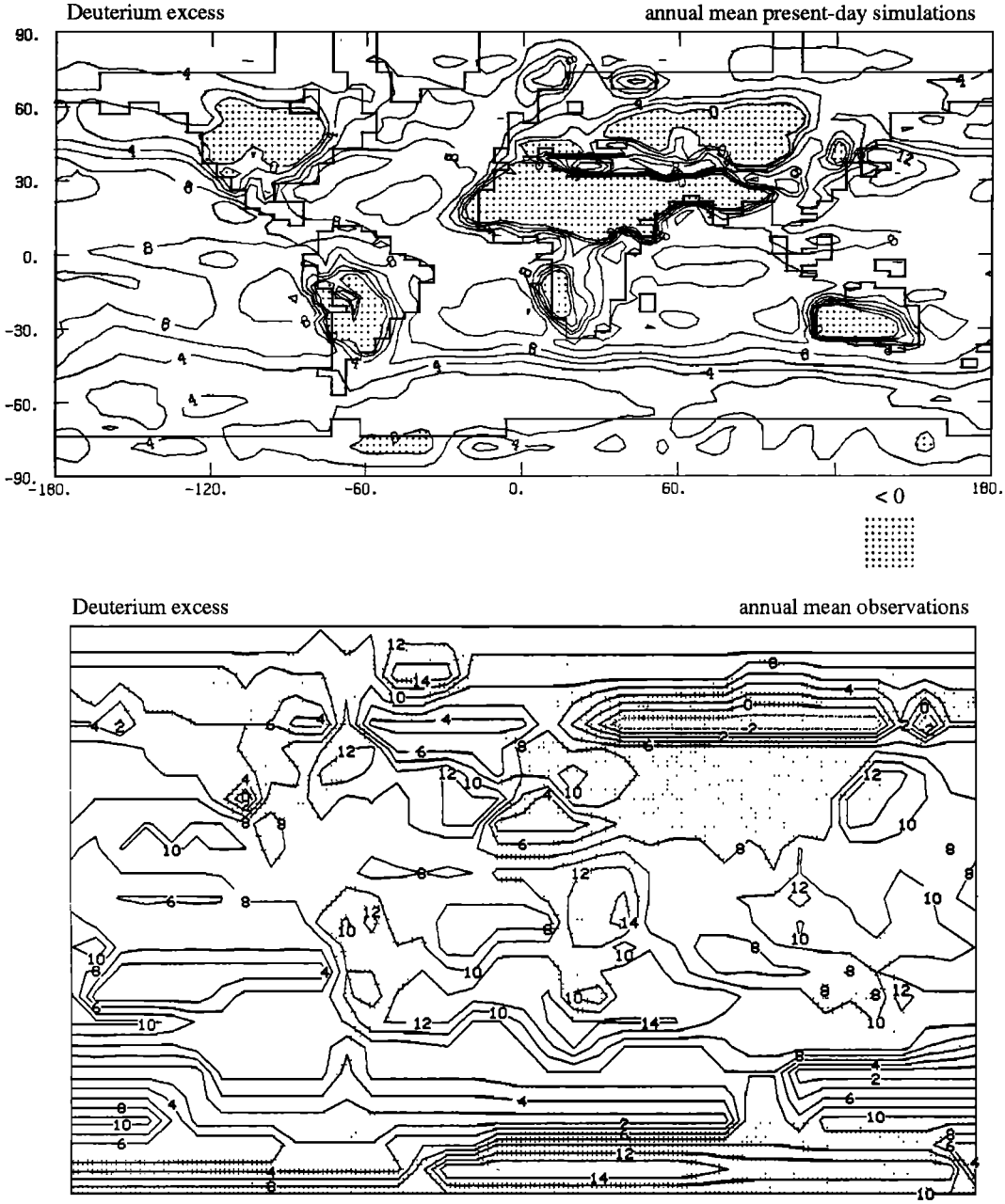

Fig. 9. Annual deuterium excess in precipitation for the present-day simulations and for observations (from *Jouzel et al.* [1987*a*]). Isolines are at every 2 ‰.

of polar isotope concentrations to transport scheme has been established through numerical experiments performed with the GISS model [*Jouzel et al.*, 1991].

7. Conclusions

For the present-day climate, the simulated atmospheric cycle of stable water isotopes is in good agreement with available observations. The simulated oxygen 18 content of precipitation correlates well with the surface air temperature field outside of tropical regions, with a mean slope of 0.7. The correlation weakens for warmer surface air temperatures, with a slope of 0.2. One of the main discrepancies between model results and observations has to do with the temperature at which the slope changes; the change occurs at about 0°C in the model and at about 15°C in observations. The origin of this discrepancy is unclear. In tropical regions, the oxygen 18 content of precipitation depends on precipitation intensity; rich ratios are produced in dry regions due to fractionation processes occurring during the reevaporation of falling rain below the cloud base.

For the simulated LGM climate, the overall patterns of the $\delta^{18}O$-temperature relationship are practically the same as those for the simulated present-day climate, both on the global and regional scale —the relationships over North America, however, do not agree. Through comparisons with paleoclimatic data, changes in the isotopic ratios of precipitation are found to be reasonably well simulated, although the model results display a higher spatial variability in East Antarctica.

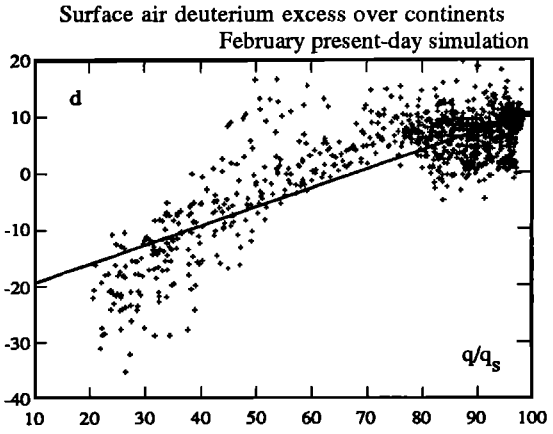

Fig. 10. The deuterium excess in precipitation over continents versus the surface air relative humidity for the present-day February simulation. The associated linear least squares fit is $d = 0.34q_1/q_s - 23.1$ (correlation coefficient, 0.81), where q_1 is computed at the first model σ layer and q_s is the saturation mixing ratio at the ground temperature T_s.

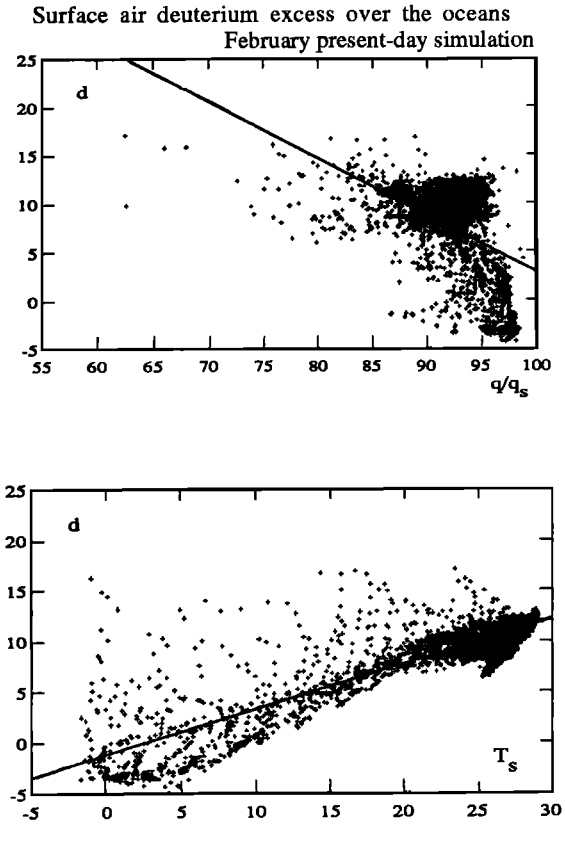

Fig. 11. The surface air deuterium excess over oceans (top) versus the surface air relative humidity and (bottom) versus the sea surface temperature, for the present-day February simulation. The associated linear least squares fits are : $d_1 = -0.59q_1/q_s + 61.8$ (correlation coefficient, -0.51) and $d_1 = 0.44T_s - 1.3$ (correlation coefficient, 0.87), where d_1 and q_1 are computed at the first model σ layer and q_s is the saturation mixing ratio at the sea surface temperature T_s.

The use of water isotopes in paleoclimatology relies on the assumption that the mean $\delta^{18}O$-temperature relationship obtained from measured present-day spatial distributions can be used to deduce time variations of temperature from measured time variations of isotopic content. The model results obtained over Greenland and Antarctica tend to corroborate this approach within error bounds of the order of 20 to 30%. However, these estimates of error bounds might be overestimated, since they result from the high spatial variability of isotopic ratios produced by the model, unlike paleoclimatic data over East Antarctica. This high variability is not only due to our very short experiments (60-day means only), since similar results are obtained over East Antarctica with the 3-year LGM and present-day simulations performed with the GISS model. This deficiency might reflect that model results deal with much shorter averaging times than ice core data do; the latter average precipitation over several decades and integrate the interannual variability of the sea surface temperature field.

While these general conclusions are corroborated by analogous experiments performed with the GISS model, some regional features do differ from one model to the other. It is important to note that simulated isotopic results may be model dependent. Sensitivity experiments, such as those performed by *Jouzel et al.* [1991], are required to examine further the use of AGCM isotope modeling in paleoclimatology.

The atmospheric circulation influences the oxygen 18 content of precipitation in the LMD model, especially through its effect on the origin of precipitating water. This mechanism produces a dispersion around the $\delta^{18}O$-temperature relationship. Therefore, persistent changes in the atmospheric circulation between glacial and interglacial climates can affect the local $\delta^{18}O$-temperature relationship. This is seen, for example, in our results over Europe.

In the model, the two water isotopes are very well correlated, in very good agreement with observations for the present-day climate. The simulated deuterium excess values in precipitation are well corroborated by present-day observations over the oceans. But over continents, the deuterium excess clearly exhibits biases compared to observations, with simulated values over dry continental areas that are too low. Over the oceans, the modeled surface air deuterium excess exhibits a clear dependence on the sea surface temperature, but a weak one on the surface air humidity. This simulated result supports the interpretation of the glacial-interglacial changes of deuterium excess over Antarctica in terms of a cooling of the sea surface temperature over the source regions of moisture. However, a comparison with paleoclimatic data indicates that too many deficiencies exist in the simulated LGM/present-day changes of deuterium excess to allow a discussion of these changes in terms of climate change.

Aside from the simulated deuterium excess, which is a second-order variable compared to isotope concentration, the model results are very promising. If these numerical experiments do not fully answer the basic questions concerning the use of water isotopes in paleoclimatology, they at least give some elements of the answers. Although the model data display a higher spatial variability than do paleoclimatic data, the model results exhibit very few changes between climates in the mean $\delta^{18}O$-temperature relationship, both on a global scale and regionally over Greenland and Antarctica. Moreover, the model allows a better understanding of the effects of the atmospheric circulation on isotope fields. While these effects are only sketched in the present study, they could be dealt more thoroughly by using the AGCM to solve simultaneously the origin of precipitating water [*Koster et al.*, 1992].

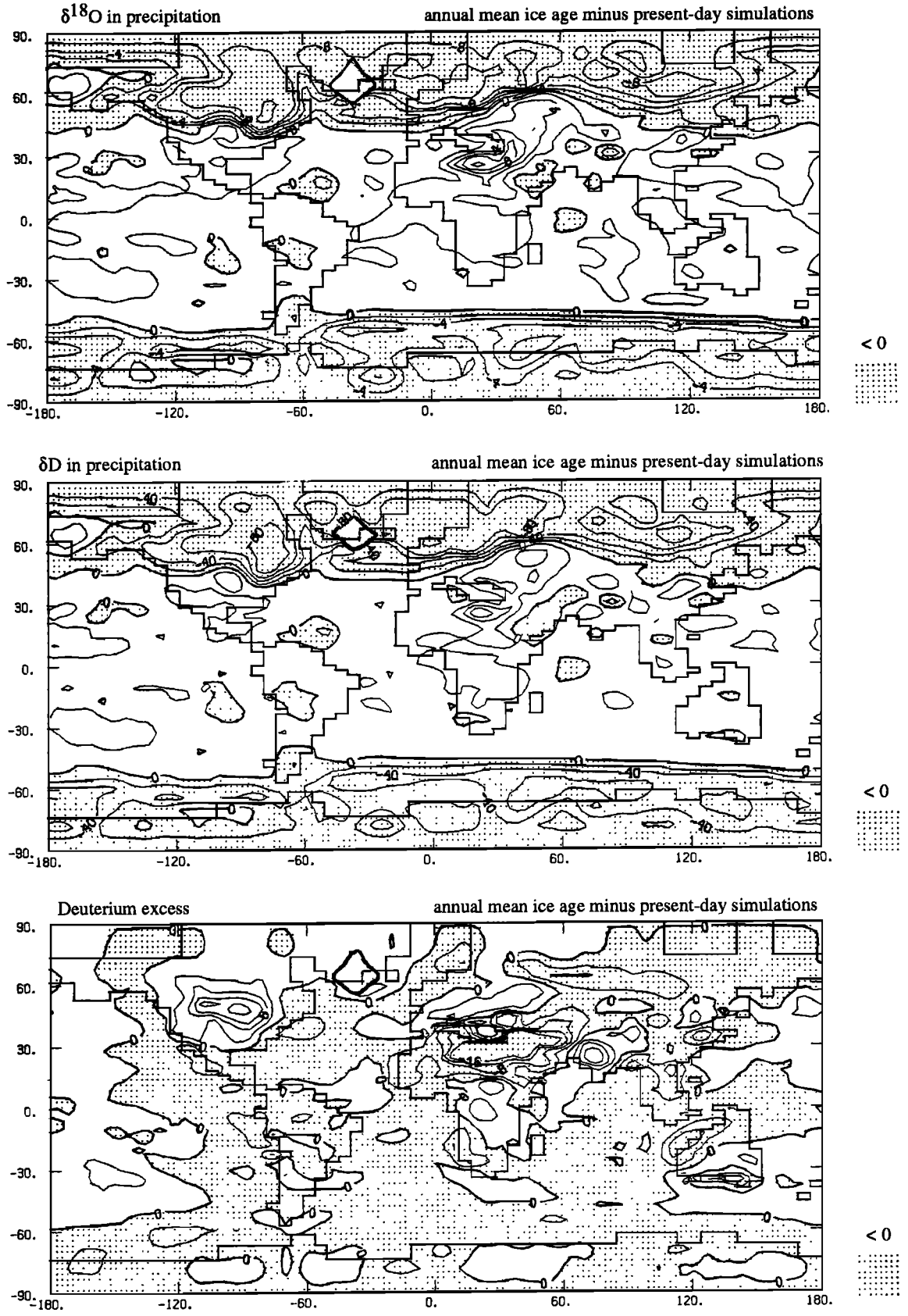

Fig. 12. The simulated ice age minus present-day change of the annual mean $\delta^{18}O$, δD and deuterium excess in precipitation. The difference values have been smoothed (Figure 4) and isolines are drawn at every 2 ‰ for $\delta^{18}O$, at every 20‰ for δD and at every 4 ‰ for the deuterium excess. Areas surrounded by a dark thick line correspond to very low precipitation rates for either the present-day or ice age climates.

TABLE 5. Comparison Between Simulated Results and Observations over Antarctica and Greenland

	Temperature, °C		Precipitation, cm/y^{-1}		$\delta^{18}O$, ‰		Deuterium Excess, ‰		Relief, m	
	Present-Day	Ice Age Minus Present-Day	Present-Day	Ice Age / Present-Day Ratio	Present-Day	Ice Age Minus Present-Day	Present-Day	Ice Age Minus Present-Day	Present-Day	Ice Age Minus Present-Day
East Antarctica, 10 Grid Point Average for the Model Results Between 78°E and 135°E										
Model results at 70°03'S	−21.4	−7.9	34.4	0.41	−25.3	−6.4	2.5	−2.5	2151	+387
Model results at 78°31'S	−32.4	−8.0	14.3	0.46	−34.1	−2.9	2.2	−0.7	3261	+477
Observations at Vostok station[1]	−55.5	≈−8	2.3	≈0.5	−57	−5			3490	
Observations at Dôme C station[2]	−53.5	≈−7	3.3	≈0.6	−49.9	−5.4	9.7	−4.5	3240	
West Antarctica, 6 Grid Point Average for the Model Results From 135°W to 101°W										
Model results at 78°31'S	−23.1	−2.8	40.5	1.37	−36.6	−0.6	3.1	0.5	1123	+993
Observations at Byrd station[3]	−28		15.8			−7			1530	
Greenland, 5 (6) Grid Point Average at 78°31'N (at 70°03'N and 64°10'N)										
Model results at 78°31'N	−10.4	−7.4	35.1	0.83	−23.8	−10.3	3.1	2.6	1048	+491
Model results at 70°03'N and 64°10'N	−9.1	−11.0	182.8	0.09	−22.4	−10.0	6.8	3.2	1798	+326
Observations at Camp Century[4]			32.	≈0.2 to 0.5	−29.	−11				
Observations at Dye 3[5]			48	≈0.6	−28	−7				

[1] Vostok station, 78°28'S and 106°48'E: *Lorius et al.*, [1985], *Jouzel et al.* [1987*b*]
[2] Dôme C station, 74°39'S and 124°10'E: *Lorius et al.* [1979], *Jouzel et al.* [1982], *Lorius et al.* [1984]
[3] Byrd station, 79°59'S and 119°31W: *Epstein et al.* [1970], *Johnsen et al.* [1972]
[4] Camp Century, 77°10'N and 61°08W: *Johnsen et al.* [1972], *Dansgaard et al.* [1969], *Beer et al.* [1988]
[5] Dye 3, 65°N and 44°W: *Dansgaard et al.* [1982], *Beer et al.* [1984], *Dansgaard and Oeschger* [1989]

TABLE 6. Comparison Between the Predicted Present-Day and Ice Age $\delta^{18}O$-Surface Air Temperature T_a and δD-$\delta^{18}O$ Relationships for the GISS AGCM (Annual Mean)

	Predicted Present-Day		Predicted Ice Age	
	Relationship	r	Relationship	r
$\delta^{18}O$–T_a relationship for $T_a < 15°C$	$0.59\,T_a - 12.7$	0.96	$0.63\,T_a - 9.9$	0.97
δD-$\delta^{18}O$ relationship	$8.06\,\delta^{18}O + 10.39$	1.0	$8.04\,\delta^{18}O + 10.64$	1.0

The correlation coefficients r are included.

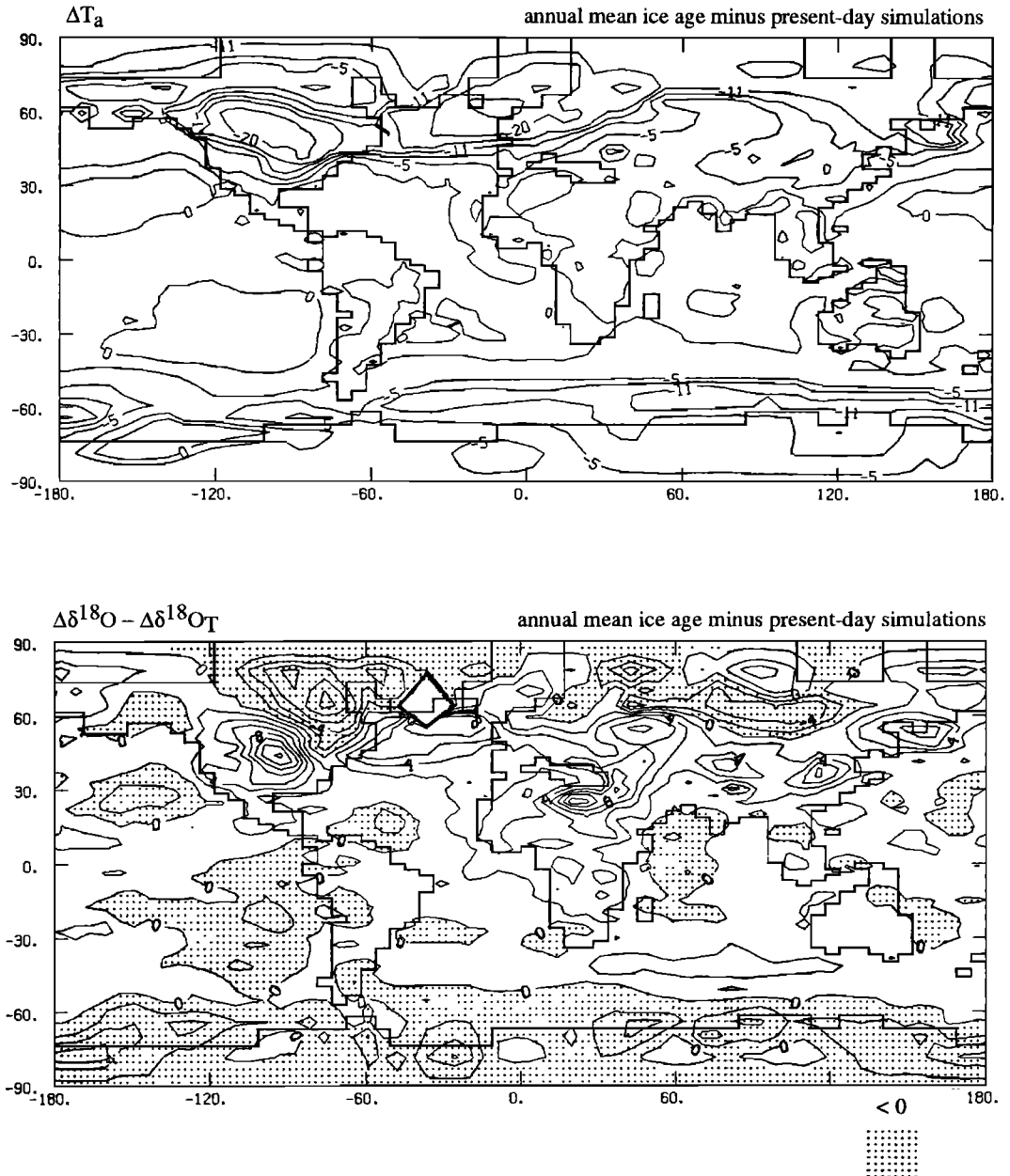

Fig. 13. The simulated ice age minus present-day change of (top) annual mean surface air temperature ΔT_a and (bottom) the shift $E = \Delta\delta^{18}O - \Delta\delta^{18}O_T$, where $\Delta\delta^{18}O_T$ is computed from ΔT_a using (7). The difference E is smoothed as in Figure 4, and isolines at every 2 ‰ are drawn. For ΔT_a, isolines are at every 3°C and correspond to isolines at every 2 ‰ for $\Delta\delta^{18}O_T$ according to (7).

TABLE 7. Same as Table 5 for the GISS AGCM

	Temperature, °C		Precipitation, cm/y^{-1}		$\delta^{18}O$, ‰		Deuterium Excess, ‰		Relief, m	
	Present-Day	Ice Age Minus Present-Day	Present-Day	Ice Age / Present-Day Ratio	Present-Day	Ice Age Minus Present-Day	Present-Day	Ice Age Minus Present-Day	Present-Day	Ice Age Minus Present-Day
East Antarctica, 5 Grid Point Average for the Model Results Between 80°E and 130°E										
Model results at 74°18'S	−46.2	−4.3	25.5	0.60	−34.6	−3.3	8.6	1.3	3118	−20
Model results at 82°12'S	−51.6	−5.1	5.0	0.58	−52.7	−9.5	11.7	6.4	3440	+465
West Antarctica, 4 Grid Point Average for the Model Results From 140°W to 100°W										
Model results at 82°12'S	−23.3	−14.6	22.5	0.91	−28.6	−6.5	4.7	4.6	1098	+1385
Greenland, 9 Grid Point Average										
Model results	−21.2	−13.4	46.1	0.42	−25.5	−5.7	11.1	−1.7	1308	+224

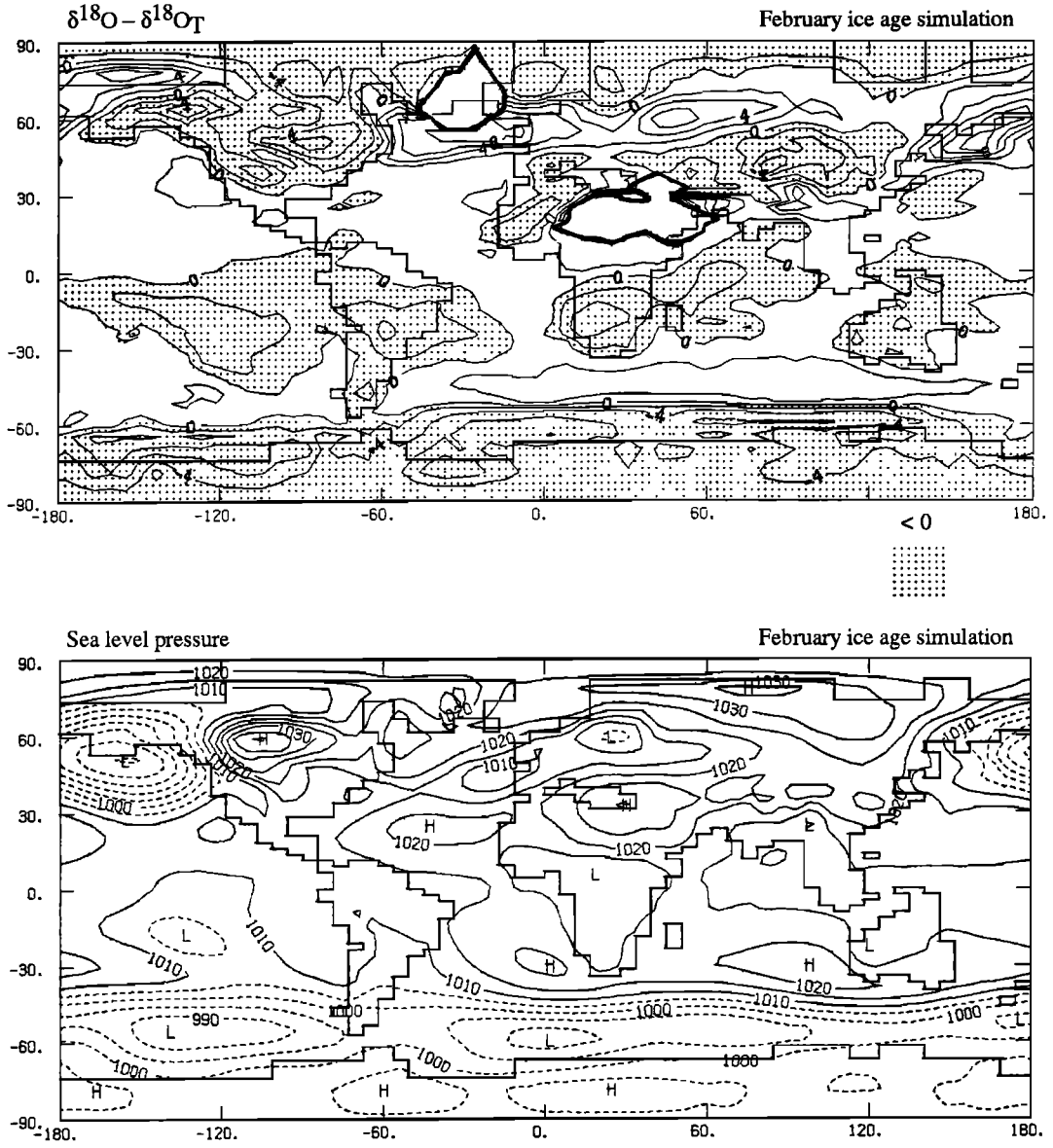

Fig. 14. The $\delta^{18}O$ shift from the annual mean temperature relationship $\delta^{18}O_T$ ($0.22T_a - 6.4$ ($T_a > 3$°C) and $0.74T_a - 8.2$ ($T_a < 3$°C)) for the simulated ice age February precipitation field, to be compared to the sea level pressure field simulated for the February ice age climate. Same isolines as in Figure 7. Areas surrounded by a dark thick line correspond to very low precipitation rates for either the present-day or ice age climates.

Acknowledgments. I thank R. Sadourny for his important contribution in the development of the dust modeling inside the LMD AGCM. I also thank G. Rabreau for his help in the development of graphics. This project was supported by the Programme National d'Etude de la Dynamique du Climat. The computing time was provided by the Centre de Calcul Vectoriel pour la Recherche. I particularly thank R. Koster, as well as B. Marsh and the anonymous referees, for their very useful comments on the text.

REFERENCES

Aristarain, A. J., J. Jouzel, and M. Pourchet, Past Antarctic Peninsula climate (1850-1980) from an ice core isotope record, *Clim. Change, 8*, 69-89, 1986.

Bath, A.H., Stable isotopic evidence for palaeo-recharge conditions of groundwater, in *Palaeoclimates and Palaeowaters: A Collection of Environmental Isotope Studies*, pp. 169-186, International Atomic Energy Agency, Vienna, Austria, 1983.

Beer, J., H. Oeschger, M. Andrée, G. Bonani, M. Suter, W. Wölfli, and C. C. Langway, Jr., Temporal variations in the ^{10}Be concentration levels found in the Dye 3 ice core, Greenland, *Ann. Glaciol., 5*, 16-17, 1984.

Beer, J., U. Siegenthaler, G. Bonani, R. C. Finkel, H. Oeschger, M. Suter, and W. Wölfli, Information on past solar activity and geomagnetism from ^{10}Be in the Camp Century ice core, *Nature, 331*, 675-679, 1988.

Craig, H., Isotopic variations in meteoric waters, *Science, 133*, 1701-1703, 1961.

Dansgaard, W., Stable isotopes in precipitation, *Tellus, 16*, 436-468, 1964.

Dansgaard, W., and H. Oeschger, Past environmental long-term records from the Arctic, in *The Environmental Record in Glaciers and Ice Sheets, Phys. Chem. Earth Sci. Res. Rep.*, vol. 8, edited by H. Oeschger and C. C. Langway, Jr., pp. 287-318, John Wiley, New York, 1989.

Dansgaard, W., S. J. Johnsen, J. Möller, and C. C. Langway, Jr., One thousand centuries of climatic record from Camp Century on the Greenland ice sheet, *Science, 166,* 377-380, 1969.

Dansgaard, W., H. B. Clausen, N. Gunderstrup, C. U. Hammer, S. J. Johnsen, P. Kristinsdottur, and N. Reeh, A new Greenland deep ice core, *Science, 218,* 1273-1277, 1982.

Duplessy, J. C., Oxygen isotope studies and Quaternary marine climates, in *Climatic Variations and Variability: Facts and Theories,* edited by A. Berger, pp. 181-192, D. Reidel, Norwell, Mass., 1981.

Epstein, S., R. P. Sharp, and A. J. Gow, Antarctic ice sheet: Stable isotope analyses of Byrd station cores and interhemispheric climatic implications, *Science, 168,* 1570-1572, 1970.

International Atomic Energy Agency, Statistical treatment of environmental isotope data in precipitation, *Tech. Rep. Ser. 206,* 253 pp., Vienna, Austria, 1981.

Johnsen, S. J., W. Dansgaard, H. B. Clausen, and C. C. Langway, Jr., Oxygen isotope profiles through the Antarctic and Greenland ice sheets, *Nature, 235,* 429-434, 1972.

Johnsen, S. J., W. Dansgaard, and J. W. C. White, The origin of Arctic precipitation under present and glacial conditions, *Tellus, Ser. B, 41,* 452-468, 1989.

Joussaume, S., Simulations du climat du dernier maximum glaciaire à l'aide d'un modèle de circulation générale de l'atmosphère incluant une modélisation du cycle des isotopes de l'eau et des poussières d'origine désertique, thèse de Doctorat d'Etat, 507 pp., Univ. of Paris VI, Paris, France, 1989.

Joussaume, S., Three-dimensional simulations of the atmospheric cycle of desert dust particles using a general circulation model, *J. Geophys. Res., 95,* 1909-1941, 1990.

Joussaume, S., Paleoclimatic tracers: An investigation using an atmospheric general circulation model under ice age conditions, 1, Desert dust, *J. Geophys. Res.,* this issue.

Joussaume, S., and J. Jouzel, Simulations of paleoclimatic tracers using atmospheric general circulation models, in *Abrupt Climatic Changes: Evidence and Implications, NATO ASI Ser. C,* vol. 216, edited by W. H. Berger and L. D. Labeyrie, pp. 369-381, D. Reidel, Norwell, Mass., 1987.

Joussaume, S., J. Jouzel, and R. Sadourny, A general circulation model of water isotope cycles in the atmosphere, *Nature, 311,* 24-29, 1984.

Joussaume, S., R. Sadourny, and C. Vignal, Origin of precipitating water in a numerical simulation of the July climate, *Ocean Air Interactions, 1,* 43-56, 1986.

Jouzel, J., Isotopes in cloud physics: Multiphase and multistage condensation processes, in *Handbook of Environmental Isotope Geochemistry, the Terrestrial Environment,* vol. 2, edited by P. Fritz and J. C. Fontes, pp. 61-112, Elsevier, New York, 1986.

Jouzel, J., and L. Merlivat, Deuterium and oxygen 18 in precipitation: Modeling of the isotopic effects during snow formation, *J. Geophys. Res., 89,* 11,749-11,757, 1984.

Jouzel, J., L. Merlivat, and C. Lorius, Deuterium excess in an east Antarctic ice core suggests higher relative humidity at the oceanic surface during the Last Glacial Maximum, *Nature, 299,* 688-691, 1982.

Jouzel, J., G. L. Russell, R. J. Suozzo, R. D. Koster, J. W. C. White, and W. S. Broecker, Simulations of the HDO and $H_2{}^{18}O$ atmospheric cycles using the NASA/GISS general circulation model: The seasonal cycle for present-day conditions, *J. Geophys. Res., 92,* 14,739-14,760, 1987*a*.

Jouzel, J., C. Lorius, J. R. Petit, C. Genthon, N. I. Barkov, V. M. Kotlyakov, and V. M. Petrov, Vostok ice core: A continuous isotope temperature record over the last climatic cycle (160,000 years), *Nature, 329,* 403-408, 1987*b*.

Jouzel, J., R. J. Suozzo, R. D. Koster, G. L. Russell, J. W. C. White, and W. S. Broecker, Simulations of the HDO and $H_2{}^{18}O$ atmospheric cycles using the NASA/GISS general circulation model: sensitivity experiments for present day conditions, *J. Geophys. Res., 96,* 7495-7507, 1991.

Koster, R. D., J. Jouzel, R. J. Suozzo, and G. L. Russell, Origin of July Antarctic precipitation and its influence on deuterium content: A GCM analysis, *Clim. Dyn., 7,* 195-203, 1992.

Kuo, H. L., On the formation and intensification of tropical cyclones through latent heat release by cumulus convection, *J. Atmos. Sci., 22,* 40-63, 1964.

Labeyrie, L. D., J. C. Duplessy, and P. L. Blanc, Variations in mode of formation and temperature of oceanic deep waters over the past 125,000 years, *Nature, 327,* 477-482, 1987.

Lorius, C., and L. Merlivat, Distribution of mean surface stable isotope values in East Antarctica; observed changes with depth in a coastal area, in Isotopes and Impurities in Snow and Ice, *IAHS AISH Publ., 118,* 127-137, 1977.

Lorius, C., L. Merlivat, J. Jouzel, and M. Pourchet, A 30,000 yr isotope climatic record from Antarctic ice, *Nature, 280,* 644-648, 1979.

Lorius, C., D. Raynaud, J. R. Petit, J. Jouzel, and L. Merlivat, Late glacial maximum-Holocene atmospheric and ice thickness changes from Antarctic ice core studies, *Ann. Glaciol., 5,* 88-94, 1984.

Lorius, C., J. Jouzel, C. Ritz, L. Merlivat, N. I. Barkov, Y. S. Korotkevich, and V. M. Kotlyakov, A 150,000 year climatic record from Antarctic ice, *Nature, 316,* 591-596, 1985.

Manabe, S., J. Smagorinski, and R. F. Strickler, Simulated climatology of a general circulation model with an hydrological cycle, *Mon. Weather Rev., 93,* 769-798, 1965.

Merlivat, L., and J. Jouzel, Global climatic interpretation of the deuterium-oxygen 18 relationship for precipitations, *J. Geophys. Res., 84,* 5029-5033, 1979.

Petit, J. R., J. W. C. White, N. W. Young, J. Jouzel, and Y. S. Korotkevich, Deuterium excess and the origin of Antarctic precipitation, *J. Geophys. Res., 96,* 5113-5122, 1991.

Phillips, F. M., L. A. Peeters, and M. K. Tansey, Paleoclimatic inferences from an isotopic investigation of groundwater in the Central San Juan Basin, New Mexico, *Quat. Res., 26,* 179-193, 1986.

Rozanski, K., Deuterium and oxygen-18 in European groundwaters -- links to atmospheric circulation in the past, *Chem. Geol., 52,* 349-363, 1985.

Rozanski, K., C. Sonntag, and K. O. Münnich, Factors controlling stable isotope composition of European precipitation, *Tellus, 34,* 142-150, 1982.

Schwarcz, H., and C. Yonge, Isotopic composition of palaeowaters as inferred from speleothem and its fluid inclusions, in *Palaeoclimates and Palaeowaters: A Collection of Environmental Isotope Studies,* pp. 115-133, International Atomic Energy Agency, Vienna, Austria, 1983.

Siegenthaler, U., and H. Matter, Dependence of $\delta^{18}O$ and δD in precipitation on climate, in *Palaeoclimate and Palaeowaters: A Collection of Environmental Isotope Studies,* pp. 37-51, International Atomic Energy Agency, Vienna, Austria, 1983.

Sonntag, C., E. Klitzsch, E. P. Löhnert, E. M. El-Shazly, K. O. Münnich, C. Junghans, U. Thorweihe, K. Weistroffer, and F. M. Swailem, Paleoclimatic information from deuterium and oxygen-18 in carbon-14 dated north Saharian groundwaters, in *Isotope Hydrology 1978,* vol. II, pp. 569-581, International Atomic Energy Agency, Vienna, Austria, 1979.

Stewart, M. K., Stable isotope fractionation due to evaporation and isotopic exchange of falling water drops: Application to atmospheric processes and evaporation of lakes, *J. Geophys. Res., 80,* 1138-1146, 1975.

Taljaard, J. J., H. van Loon, H. Crutcher, and R. L. Jenne, Climate of the upper air: Southern hemisphere, vol. 1, Temperatures, dew points and heights at selected pressure levels, *NAVAIR Publ. 50-1C-55,* Nav. Weather Serv. Command, Washington, D. C., 1969.

Yapp, C. J., and S. Epstein, Climatic implications of D/H ratios of meteoric water over North America (9500-22,000 BP) as inferred from ancient wood cellulose C-H hydrogen, *Earth Planet. Sci. Lett., 34,* 333-350, 1977.

Yurtsever, Y., and J. Gat, Atmospheric waters in stable isotope hydrology, deuterium and oxygen 18 in the water cycle, *Tech. Rep. Ser. 210,* pp. 103-142, Int. At. Energy Agency, Vienna, Austria, 1981.

S. Joussaume and J. Jouzel, Laboratoire de Modélisation du Climat et de l'Environnement, Direction des Sciences de la Matière, Batiment 709, Centre d'Etudes de Saclay, 91191 Gif sur Yvette, France.

(Received June 4, 1991;
revised July 24, 1992;
accepted August 10, 1992.)